Rock fracture characteristics regulate water storage and seasonal tree water uptake in karst~~The role of rock fractures on tree water use of water stored in bedrock: Mixing and residence times~~

Xiuqiang Liu[1], Xi Chen[1,2], Zhicai Zhang[3], Weihan Liu[1], Tao Peng[4,5], Jeffrey J. McDonnell[6,7,8]

[1]School of Earth System Science, Institute of Surface-Earth System Science, Tianjin University, Tianjin 300072, China
[2]Tianjin Key Laboratory of Earth Critical Zone Science and Sustainable Development in Bohai Rim, Tianjin University, Tianjin 300072, China
[3]College of Hydrology and Water Resources, Hohai University, Nanjing 210098, China
[4]State Key Laboratory of Environmental Geochemistry, Institute of Geochemistry, Chinese Academy of Sciences, Guiyang 550081, China
[5]Puding Karst Ecosystem Research Station, Chinese Academy of Sciences, Puding 562100, China
[6]Global Institute for Water Security, School of Environment and Sustainability, University of Saskatchewan, Saskatoon, Saskatchewan, Canada
[7]North China University of Water Resources and Electric Power, Zhengzhou, China
[8]School of Geography, Earth and Environmental Sciences, University of Birmingham; Birmingham, UK.
Corresponding to: Xi Chen (xi_chen@tju.edu.cn)

Abstract. The processes of tree water uptake in karst environments are poorly understood. One of the main challenges to improved understanding is the complex interaction between soil water and bedrock water, especially in systems characterized by structurally heterogeneous rock fractures. While some studies have highlighted the potential importance of fractured bedrock as a water source for plants, few have quantitatively assessed how fracture characteristics regulate water storage, residence times, and plant water uptake across seasons.~~the sources, residence times, and seasonal dynamics of tree water uptake from both soil and rock fracture compartments.~~ Here, we combine stable isotope tracing, a Bayesian mixing model (MixSIAR), and hydrometric monitoring to quantify the contributions and mean residence times (MRT) of soil and rock water accessed by trees as a function of fracture properties~~across seasons~~. We use a four-compartment sampling framework that distinguishes between soil water (mobile and bulk) and rock water (fracture and infilled fracture). Our results show that fracture characteristics exert a primary control on seasonal tree water uptake patterns. ~~reveal clear seasonal shifts in plant water sourcing: during~~ During the peak growing~~rainy~~ season, mobile soil water (mean MRT = 88 days) dominates uptake (mean contribution 41%), whereas in late growing season, trees increasingly rely on bulk soil water (mean MRT = 95 days, mean contribution 55%). During the transition from the dry to the wet season, reliance on rock water increased in fracture-rich areas. In the reactivation stage, trees exhibited a mean rock-water contribution of 69% (mean MRT = 117 days), and in the subsequent early growing season, large trees derived up to 85% of their water from rock, primarily from soil-filled fractures with apertures >10 mm that act as seasonal storage reservoirs with prolonged residence times (MRT = 84 – 303 days). ~~Strikingly, in early spring, trees in fracture-rich areas exhibit the highest reliance on rock water (mean MRT = 113 days, mean contribution 69%). During the subsequent early growing season, large trees derive up to 85% of their water from rock, particularly from soil-filled fractures with apertures >10 mm, which act as transitional reservoirs capable of retaining precipitation for extended periods~~

~~(MRT = 84-303 days).~~ Trees preferentially access short-MRT sources under wet conditions and shift to longer-MRT pools during dry periods, demonstrating that seasonal water-use strategies are strongly regulated by fracture-controlled storage and connectivity~~reinforcing the concept of ecohydrological separation between tightly bound and dynamically recharged water pools. However, this separation is attenuated during periods of high precipitation due to increased hydraulic connectivity and water mixing.~~. This study demonstrates that fracture characteristics play a central role in regulating rock water storage and tree water uptake in karst systems, providing new insights into vegetation resilience in structurally complex landscapes and implications for water resource management under changing climatic conditions.~~This work advances our understanding of vegetation resilience in structurally complex and hydrologically dynamic karst landscapes with important insights for sustainable water resource management under changing climatic conditions.~~

设置了格式: 字体: (默认) Times New Roman

1 Introduction

Water transport and retention are critical for understanding the hydrodynamic behavior of the soil-plant-atmosphere continuum, in which the transfer of water through the plant and soil is a central process (Deng et al., 2017; Philip, 1966). Climate and critical zone regimes influence how plants access and utilize water resources by modulating precipitation inputs, root zone water transit, and residence times (Liu et al., 2024c; Luo et al., 2023; Fan and Miguez-Macho, 2024). Consequently, the temporal dynamics of water transport within trees directly influence ~~The time it takes for water to be transported within trees can affect~~ how forests store and release water, thereby altering the timing and magnitude of water fluxes such as transpiration and runoff at the ecosystem scale (Bond et al., 2008).

Stable isotopes of hydrogen and oxygen (^{2}H and ^{18}O) have been powerful tracers for quantifying water transport (Putman and Bowen, 2019). When combined with isotope-based models, such as linear mixing models (IsoSource, SLM), Bayesian mixing models (SIAR, MixSIR, and MixSIAR), and continuous distribution models (e.g., CrisPy), the relative contributions of each water source to plant water use can be quantified (Wang et al., 2019a; Fu et al., 2024; Putman and Bowen, 2019). However, beyond mere source attribution, quantifying the temporal dynamics of water movement is essential for characterizing subsurface storage. Metrics such as Mean Residence Time (MRT) and Mean Transit Time (MTT) have been widely employed to estimate catchment water storage durations and the temporal lag between precipitation input and plant uptake (McGuire et al., 2002; Asadollahi et al., 2020; Liu et al., 2024c). While MRT reflects the storage capacity and mixing volume of a reservoir, and MTT characterizes the transport velocity, their application in complex karst environments remains challenging. Unlike homogeneous soils where these methods are effective (Liu et al., 2024c; Stewart and McDonnell, 1991), the high heterogeneity of karst fracture networks creates a dual-domain system characterized by rapid conduit flow and slow matrix storage. This complexity confounds standard residence time estimations (Hartmann et al., 2014; Zhang et al., 2021). Nevertheless, applying MRT and MTT analysis to specific karst water pools (e.g., fracture vs. matrix) offers a unique opportunity to unravel the temporal disparities that drive plant water availability.

~~These~~ Conventionally, isotope tracing tools have been applied to identify when and where soil water is accessed by plants~~tools have been widely applied to identify when and where soil water is accessed by plants~~ (Midwood et al., 1998; Tang

and Feng, 2001; McCole and Stern, 2007; Darrouzet-Nardi et al., 2006; Wang et al., 2010; Brooks et al., 2010). Recent advances have crystallized into~~introduced~~ the "ecohydrological separation hypothesis", which posits that water contributing to plant transpiration is often distinct from the water that generates runoff or groundwater recharge (McDonnell, 2014; Brooks et al., 2010). This framework suggests the coexistence of at least two functionally distinct water reservoirs within the soil: a mobile, hydrologically connected fraction and a more strongly bound, plant-available fraction (Sprenger and Allen, 2020; Finkenbiner et al., 2022). However, empirical evidence for ecohydrological separation stems predominantly from soil-dominated ecosystems. In karst landscapes, the "soil" layer is often shallow and discontinuous, implying that separation mechanisms may fundamentally differ due to the underlying fractured bedrock. It remains unclear whether the ecohydrological separation hypothesis applies to the coupled soil-rock continuum, where the disparity between rapid fracture flow and water retained in soil-filled crevices could create a distinct form of separation critical for vegetation survival.

Following the seminal works of ~~However, beginning with work of~~ Salve et al. (2012) and Oshun et al. (2016) increasing attention has been directed toward ~~given to~~ a third, hidden water reservoir: rock moisture, defined as~~which refers to~~ water stored in unsaturated weathered bedrock (Zhang and Zhang, 2021; Rempe and Dietrich, 2018). This water often exists at matric potentials above the turgor loss point of roots (> -1.5 MPa) (Korboulewsky et al., 2020; Nardini et al., 2021; Zwieniecki and Newton, 1996; Schoeman et al., 1997; Hubbert et al., 2011). Under prolonged drought conditions ~~in certain environments~~, plants in specific environments are known to ~~can~~ shift their water use strategy from shallow soil water to this deeper rock water (Ning et al., 2023; Jiménez-Rodríguez et al., 2022; Barbeta et al., 2015; Hahm et al., 2022; Nardini et al., 2024). Despite significant progress in delineating the geographical extent and importance of rock moisture ~~But while considerable progress has been made in understanding the role of rock moisture and its geographical extent~~ (McCormick et al., 2021), the mechanisms of its extraction remain elusive. Since much of the weathered rock zone is fractured, few studies have quantified the specific contribution of rock fracture water to plant uptake.~~the mechanisms of rock moisture extraction are still poorly understood. Since much of the weathered rock zone is fractured, few if any studies have quantified the role of rock fracture water in plant water sourcing from rock moisture.~~

It is well established that ~~We know that~~ plant roots have the ability to access rock water in fractures (Schwinning, 2020). Studies suggest that the minimum fracture aperture required for root water uptake is approximately 0.1 mm (Zwieniecki and Newton, 1995; Schwinning, 2010). Once this threshold is exceeded, capillary forces diminish, while both hydraulic conductivity and volumetric flow increase significantly with fracture aperture (Liu et al., 2024b; Wang et al., 2015; Zimmerman and Bodvarsson, 1996; Wang et al., 2022). These hydraulically active microfractures can establish water connectivity across fracture networks (Wolfsberg, 1997), forming dynamic reservoirs (Jiménez-Rodríguez et al., 2022; Ning et al., 2023; Vrettas and Fung, 2017), that enhance the likelihood of plant access to rock moisture (Schwinning, 2020, 2010). Moreover, these fractures can act as sheltered conduits for root extension, buffering roots against environmental extremes such as thermal fluctuations and wind exposure, while their enclosed structure reduces evaporative losses, allowing water to be retained for longer periods (Pawlik et al., 2016; Zhang et al., 2016; Preisler et al., 2019; Hahm et al., 2020; Luo et al., 2024a). This protective effect allows roots to penetrate deep into the substrate and access water and nutrients that are inaccessible in shallow

设置了格式: 字体: 非加粗

soils (Zhang et al., 2019a). Notably, ~~In many cases,~~ larger fractures may become partially or fully filled with soil, further enhancing their capacity to retain water and provide nutrients to vegetation (Liu et al., 2024b; Peng et al., 2019; Estrada-Medina et al., 2013; Yang et al., 2016).

However, the mechanistic controls underlying plant water uptake from different fracture types remain poorly understood. Plants growing on different rock substrates may access varying amounts of available water, depending on the physical properties of the underlying fractures (Nardini et al., 2021; Querejeta et al., 2006; Zwieniecki and Newton, 1996; Nardini et al., 2024). No study that we are aware of has yet systematically examined how fracture aperture, depth, and degree of soil infill influence both the residence time of stored water and the patterns of plant water uptake. We propose that these static physical characteristics of fractures are the primary drivers of dynamic seasonal shifts in plant water use. Rather than viewing seasonal variation solely as a climatic response, we argue that the structural heterogeneity of fractures (e.g., aperture and infill) dictates the temporal availability of water (residence time), thereby forcing plants to shift sources as different reservoirs fill or deplete at different rates. These structural attributes may determine whether a fracture functions as a fast conduit, a temporary buffer, or a long-term reservoir for plant-available water.

In this study, we conduct~~Here we conduct~~ a systematic and mechanistic examination of the role of rock fractures on tree water use of water stored in bedrock. By incorporating ~~We include~~ within-fracture measurements and sampling~~,~~ , we target a representative ~~and focus on a~~ karst landscape. In such karst environments, ~~,~~ the epikarst serves as a pivotal hydrological interface between surface and subsurface systems, potentially regulating water storage, transmission, and plant growth~~epikarst has been shown to play a pivotal role as a hydrological interface between surface and subsurface systems and potentially regulates water storage and transmission, as well as plant growth~~ (Wang et al., 2022). Epikarst thickness typically ranges ~~Epikarst is known to range~~ from 0.5 to 30 meters (Williams, 2008), and its highly developed pore and fracture networks not only facilitate the transformation of surface water into groundwater but also provide growth pathways for plant roots to access deep rock fractures. We focus on a site in southwest China's karst region, characterized by a subtropical monsoon climate. Ecologically, the site is dominated by mixed evergreen and deciduous broad-leaved secondary forests, which represent the typical vegetation recovery following karst rocky desertification in this region. Beyond its specific karst features, the Puding station serves as a natural laboratory for studying hydrological processes in shallow-soil, fractured-bedrock ecosystems globally. The site typifies complex Critical Zones where regenerating vegetation grows on thin, discontinuous soils overlie highly permeable bedrock (Zhang et al., 2019b; Jiang et al., 2020), ultimately increasing the frequency of drought events (Xu et al., 2023; Wang et al., 2019b)~~.~~. This bio-geological structure mirrors not only Mediterranean carbonate terrains but also other fractured rock environments where vegetation relies on rock moisture to survive seasonal drought~~. We focus on a site in southwest China's karst region that is characterized by a subtropical monsoon climate with distinct seasonality.~~(Wang et al., 2019b; Chen et al., 2011; Carrière et al., 2020). ~~Here summer precipitation is abundant, the shallow soil layer, often less than 50 cm thick, but the high permeability of the fracture network result in rapid water percolation and shortened residence times of moisture within fractures (Zhang et al., 2019b; Jiang et al., 2020), ultimately increasing the frequency of drought events (Xu et al., 2023; Wang et al., 2019b).~~ Despite the hydrological challenges, the structure of the soil-rock system can modulate

域代码已更改
域代码已更改
域代码已更改
域代码已更改

local water storage; in areas where the epikarst possesses stronger water-holding capacity, the combined soil-fracture system retains both water and nutrients, offering critical support to maintaining the stability and sustainability of these ecosystems~~Nevertheless, the structure of the soil-rock system can modulate local water storage and availability. In areas where the epikarst has a stronger water-holding capacity, the combined soil-fracture system can retain both water and nutrients, offering critical support to karst ecosystems and maintaining their stability and sustainability~~ (Wang et al., 2024b). However, the mechanistic extent to which this structural heterogeneity within the fractured bedrock dictates the partitioning of subsurface water resources and subsequently drives the water uptake patterns and survival of the overlying vegetation remains to be systematically unraveled.

We hypothesize that subsurface partitioning may extend beyond the soil matrix to include fractured bedrock, where water is stored in forms ranging from fast-draining open fissures to long-residence, soil-filled fractures. Although these subsurface compartments are hydraulically connected, they may differ substantially in renewal rates, retention times, and plant accessibility, effectively forming a structurally and functionally analogous extension of ecohydrological separation. This study aims to provide a scientific foundation for sustainable water resource management and vegetation restoration in karst environments. Specifically, this study will address three fundamental research questions:

1. How do rock fractures (aperture size, filling conditions, hydraulic properties) regulate the temporal availability of water and subsequently drive the~~affect~~ water uptake patterns of plant roots?
2. What factors influence the residence time and transit times in soil, rock and plant water system in karst?
3. To what extent does ecohydrological separation occur in this coupled soil-rock system and what does~~and~~ seasonal rainfall plays in shaping this separation?

To address these questions, we use a sampling approach where soil water is subdivided into mobile water (sampled via lysimeters) and bulk water (sampled via cryogenic extraction), while rock water comprises rock fracture water and infilled rock fracture water. This enabled us to distinguish among four types of water sources: mobile soil water, defined as water residing in connected soil pores that responds rapidly to rainfall events; bulk soil water, defined as more tightly bound water in micropores, characterized by slower renewal and longer retention; rock fracture water: defined as water stored in clean, unfilled fractures within weathered bedrock, often transient and dynamic and infilled rock fracture water, defined as water held in fractures partially or fully filled with soil, offering higher retention and potential nutrient supply.

2 Material and methods

2.1 The study area and sampling location

Our experimental site is located at the Puding Karst Ecosystem Research Station in Guizhou, southwest China (105°42'-105°43'E, 26°14'-26°15'N) (Fig. 1). The climate is dominated by subtropical humid monsoon. The mean annual temperature is 15.1℃, and the mean annual precipitation is 1378 mm. Precipitation in this region occurs exclusively in the form of rainfall. Over 80% of annual precipitation occurs from May to October as summer rainfall (Liu et al., 2022). The carbonate rocks consist mainly of limestone. Soils developed from black and yellow limestone are distributed irregularly across the study site

(Li et al., 2023) with soil-filled 'grykes' (i.e. cracks that form vertically in the limestone via chemical weathering, Parry (1960)) widely distributed (Fig. 1). The thickness of the root-zone soil ranges from 15 cm to 200 cm (mean: 66 cm), the bare rock coverage varies from 0.42 to 0.94, and the apertures of rock fractures range from 0.1 mm to 38 mm (mean: 2.4 mm), with over 70% of fractures having apertures narrower than 1 mm. Fractures with apertures greater than 10 mm are often completely or partially filled with soil (Liu et al., 2024b; Liu et al., 2025). The vegetation at the site consists of secondary broadleaf forests that have regenerated after environmental disruption caused by human activities, such as deforestation for cultivation.

We selected five typical sites (A-E in Fig. 1) to survey the soil-rock structure and tree stand structure (Liu et al., 2025). The five sites included 18 individual trees of 5 different species, including deciduous broadleaf trees (*Broussonetia papyrifera* (L.) L'Hér. ex Vent. (bp_{1-5}), *Koelreuteria paniculata* Laxm. (kp_{1-2}), *Toona sinensis* (A.Juss.) M.Roem. (ts_{1-6}), and *Yulania denudata* (Desr.) D.L.Fu. (yd_{1-6})), and one evergreen broadleaf tree (*Cinnamomum camphora* (L.) J.Presl. (cc_{1-3})).

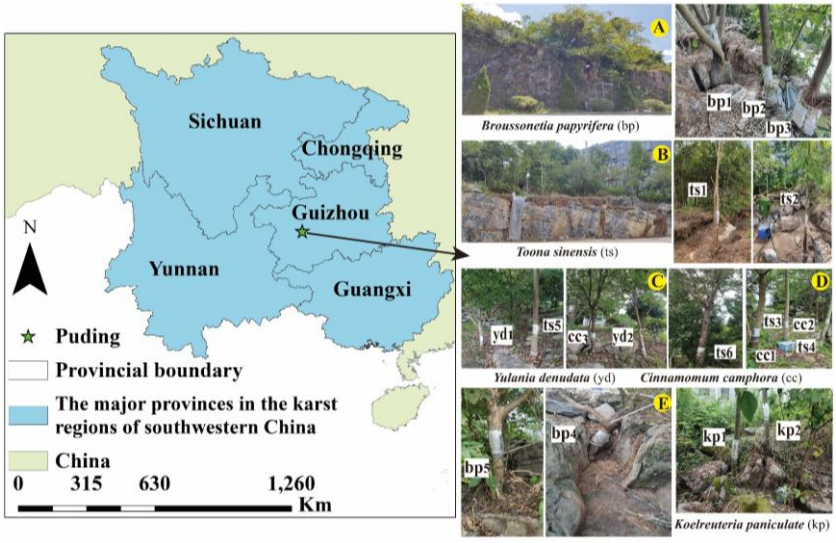

Figure 1. The study area and five sampling sites.

2.2 Field measurements

2.2.1 Collecting samples for isotope analysis

The method for collecting mobile soil water and bulk soil water samples at different depths involved two preparatory steps: (1) soil boreholes were manually drilled using a soil auger to predefined discrete depths at each study site ~~Using a soil auger, we manually drilled soil boreholes to depths of 0.1 to 2 m~~; (2) at selected depths, soil material was removed and ceramic tensiometer tips connected to suction lysimeters were installed for the collection of mobile soil water. ~~At each target depth, soil was removed, and ceramic tensiometer tips connected to suction lysimeters were inserted.~~ The boreholes were then backfilled

with the original soil to ensure proper contact and minimize disturbance. Bulk soil samples were collected at all predefined depths and bulk soil water was subsequently extracted from the collected soil samples using laboratory extraction methods. The site-specific sampling depths, sampling frequency, and sampling periods for bulk soil water and mobile soil water are summarized in Table A1.~~Bulk soil water was extracted from the collected soil samples through laboratory extraction.~~

Following the conceptual framework of Sprenger et al. (2018), we distinguish between mobile soil water and bulk soil water based on their retention characteristics and accessibility under different matric suctions. Mobile soil water refers to the fraction of soil water that is weakly retained in the soil matrix and occupies larger, well-connected pores, making it accessible at relatively low matric suction and responsive to recent precipitation inputs. In this study, bulk soil water was sampled at least two days after rainfall, when gravitational water had largely drained from the soil profile. Under these conditions, the extracted bulk soil water was dominated by more strongly retained, matrix-bound water, with only a minor contribution from mobile water. To operationalize this conceptual distinction, soil water retention curves were constructed for each site and soil layer based on previously established soil hydraulic parameters (Liu et al., 2024b). Based on soil moisture distribution characteristics, site- and depth-specific upper suction thresholds associated with mobile soil water were identified for different soil types. The estimated maximum suction values corresponding to mobile soil water varied across sites and depths, reflecting differences in soil texture and hydraulic properties. Specifically, upper suction thresholds ranged from approximately 70–90 kPa at Site A (50–100 cm), 65–90 kPa at Site B (20–180 cm), 40–45 kPa at Sites C and D (20–50 cm), and 55–80 kPa at Site E. During field sampling, mobile soil water was collected using suction lysimeters operated at vacuum pressures below these site- and depth-specific upper suction thresholds to ensure that the extracted water predominantly represented mobile soil water rather than tightly bound soil water.

~~To determine the suction range corresponding to mobile soil water, this study constructed soil water retention curves based on previously established soil hydraulic parameters (Liu et al., 2024b). According to the soil moisture distribution characteristics, the mobile water content range and its corresponding maximum suction for different soil types were identified. The results indicate that the maximum suction range of mobile water at different sample sites is as follows: Site A: 70–90 kPa, Site B: 65–90 kPa, Sites C&D: 40–45 kPa, and Site E: 55–80 kPa. Therefore, during the actual extraction of mobile soil water, it is necessary to set the applied vacuum values appropriately based on the hydraulic characteristics of different soil layers, ensuring that they are below the maximum suction range of mobile water. This practice ensures that the collected water mainly originates from mobile soil water, avoiding excessive extraction of bound water, thus enhancing the representativeness and accuracy of the sampling. This method is also consistent with the findings of Sprenger et al. (2018), who noted that mobile soil water collected by vacuum samplers typically corresponds to a maximum suction of about 60 kPa.~~

~~Bulk soil water was extracted from the collected soil samples through laboratory extraction.~~

~~For the collection of rock fracture water, 26 representative fracture locations were selected based on prior field investigations (Liu et al., 2024b). At each location, boreholes were drilled and rock cores were extracted using a portable core drilling tool. We inserted the ceramic tensiometer tips with PVA sponges into the boreholes so that the ceramic tips were located~~

~~at the fractures where water samples needed to be collected. We used sponges to isolate other fracture layers to prevent mixing of fracture water from different depths. The ceramic tips in the soil and fractures were connected to sampling bottles, and a vacuum pump was used to create a negative pressure in the sampling bottles to collect rock water.~~ Rock fracture water and infilled rock fracture water were distinguished based on fracture aperture and the presence of infill material observed during drilling and coring. Fractures with apertures ranging from approximately 0.1 to 10 mm generally exhibited minimal soil or sediment infill and were therefore considered to predominantly store free fracture water. Water collected from these fractures is referred to as rock fracture water. In contrast, fractures with apertures larger than approximately 10 mm were commonly partially or fully filled with soil or fine sediments. Water collected from these zones primarily represents water stored within infilled fracture material and is referred to as infilled rock fracture water. For the collection of fracture water, 26 representative fracture locations were selected based on prior field investigations (Liu et al., 2024b). At each location, boreholes were drilled and rock cores were extracted using a portable core drilling tool to directly identify fracture geometry, aperture, and infill conditions. Ceramic tensiometer tips connected to suction samplers were positioned directly within the targeted fracture zones according to the fracture classification described above. To prevent mixing of water from fractures at different depths, PVA sponges were used to hydraulically isolate individual fracture layers within the boreholes. The ceramic tips installed in soil and fracture zones were connected to sampling bottles, and a vacuum pump was used to apply negative pressure for water extraction (Fig. A1). The site-specific sampling depths, fracture apertures, sampling frequency, and sampling periods for rock fracture water and infilled rock fracture water are summarized in Table A2.

At each study site, representative trees were selected for xylem water sampling. Tree physiological traits and root-zone soil-rock structural characteristics are summarized in Table A3. More detailed information on vegetation characteristics and root-zone soil-rock structure at the study sites is provided in Liu et al. (2025). For each sampling campaign, three branches were collected from different positions of each sampled tree to provide within-tree replication. Sampling was conducted from September 2022 to March 2024, with an average sampling frequency of approximately two to three times per month. The bark and phloem were removed immediately after sampling, retaining only the xylem tissue, and samples were promptly sealed in airtight containers prior to laboratory analysis.~~For collecting tree branch samples we removed the bark, keeping only the xylem, and sealed them promptly.~~

Precipitation samples were collected during individual rainfall events using a standard precipitation collector installed at 1.5 m above ground level to minimize splash contamination and evaporation effects. The collector was placed in an open area, away from buildings and vegetation, to avoid external contamination. From September 2021 to March 2025, a total of 182 precipitation samples were collected.

All soil and xylem samples were stored frozen, while soil water, ~~fracture~~ rock water, and rainwater samples were refrigerated for storage.

~~From September 2022 to March 2025, samples were collected at an average frequency of 1–3 times per month.~~

设置了格式: 字体颜色: 文字 1

设置了格式: 字体颜色: 文字 1

设置了格式: 字体颜色: 文字 1

2.2.2 Moisture and sap flow monitoring

Meteorological variables were observed at the standard meteorological station of the Puding Karst Ecosystem Research Station. Automatically recorded variables included precipitation (P), air temperature at 2 m height (T_a), and soil moisture content at depths of 0–200 cm at each sampling site, monitored using capacitance-based frequency domain reflectometry (FDR) sensors (5TM, METER Group, Pullman, WA, USA) at 30 minute intervals. Additional sensors at various depths were also installed at the soil-rock interface profiles at sites A and B. Detailed procedures for monitoring rock moisture content and sap flow in trees are described in (Liu et al., 2025).

2.3 Laboratory analyses

Due to the long-term nature of the project and the development of international collaboration, sample processing and testing were divided into two analytical periods. Samples collected between September 2022 and March 2024 were processed and analyzed at the Ecohydrology and Water Resources Research Center and the Experimental Test Analysis Science and Technology Center, School of Earth System Science, Tianjin University. Samples collected from April 2024 to March 2025 were processed and analyzed at the University of Saskatchewan, Canada. ~~Sample processing and testing were divided into two periods. Samples collected from September 2022 to March 2025 were processed and analyzed at the Ecohydrology and Water Resources Research Center and the Experimental Test Analysis Science and Technology Center of the School of Earth System Science at Tianjin University.~~

To collect xylem water from vegetation, the collected arboreal branches were processed using the LI-2100 fully automatic vacuum condensation extraction system (Beijing Ligajoint Scientific Co., Ltd., China) to extract liquid water (cryogenic vacuum distillation technique, CVD). Prior to extraction, the samples were weighed with a microbalance (accuracy of 0.1 mg), and the heating temperature for extraction was set to 150°C with a duration of three hours. After extraction, the samples were weighed again to calculate the volume of water extracted, and then dried at 105°C for 24 hours. The dry samples were weighed again to calculate the total water loss, and the water extraction rate was calculated based on the weight loss (the proportion of water extracted to the total water loss after drying). The water extraction rate for all samples was generally above 99%. Samples with less than 99% water extraction rate were re-extracted until the standard was met.

Water isotopes δD and $\delta^{18}O$ in rainfall, mobile soil water, and rock water samples were measured using the Picarro L2140-i water isotope analyzer. The measurement errors for δD were 0.1‰, and for $\delta^{18}O$ were 0.015‰. As tree branch water contains volatile organic compounds (VOCs), all plant extracted waters were analyzed using the MAT 253 Plus gas stable isotope ratio mass spectrometer to determine δD and $\delta^{18}O$ values. The errors for δD were 2‰, and for $\delta^{18}O$ were 0.2‰.

Samples from April 2024 to March 2025 were processed and analyzed at the University of Saskatchewan in Canada.

Water was extracted from plant xylem and soil samples using the CVD method developed by Koeniger et al. (2011). After freezing the sample vials with liquid nitrogen, they were connected via a capillary tube to a collection vial, vacuumed to below 0.8 mbar, and heated at a predetermined temperature for a specified duration. In this closed system, vaporized water from the sample vial was condensed into the collection vial. The extracted water was then transferred to 2 mL screw-cap glass vials.

Extracted samples were subsequently oven-dried at 105 °C for 24 hours to evaluate extraction efficiency. Plant samples were extracted at 200 °C for 24 minutes, while soil samples were extracted at the same temperature for 30 minutes (Wang et al., 2024a). Higher extraction temperatures and efficient water recovery help to minimize isotope ratio errors in soil and xylem water samples (Younger et al., 2024).

Rainfall, mobile soil water, and rock water samples were analyzed using an Off-Axis Integrated Cavity Output Spectroscopy (OA-ICOS) system from Los Gatos Research, with post-processing performed via the LIMS for Lasers 2015 software. Due to the presence of organic compounds in plant and soil-extracted water samples, these were analyzed using isotope ratio mass spectrometry (IRMS). For hydrogen isotope analysis, the elemental analyzer-IRMS (EA-IRMS) method was employed, where water samples reacted with elemental chromium at high temperatures to produce hydrogen gas, following the method of Morrison et al. (2001). The resulting hydrogen gas was separated using a gas chromatographic column and then analyzed by IRMS. For oxygen isotope analysis, the CO_2-H_2O equilibration method described by Epstein and Mayeda (1953) was used Epstein and Mayeda (1953), wherein water equilibrates with CO_2 at a controlled temperature and the isotopic composition of the equilibrated CO_2 is then measured by IRMS.

The analytical uncertainties (2σ) for LGR measurements of liquid samples~~for δD, $\delta^{18}O$, and $\delta^{17}O$~~ were ± 2‰~~,~~ and ± 0.8‰ for δD, $\delta^{18}O$~~, and ± 0.5‰~~, respectively. Water extracted from soil and plant samples was analyzed using isotope ratio mass spectrometry (IRMS). The analytical precision of IRMS was approximately~~Laboratory reproducibility was~~ ± 1.0‰ for δD and ±0.2‰ for ~~both~~ $\delta^{18}O$ ~~and $\delta^{17}O$~~. All isotope values were reported in per mil (‰) relative to the Vienna Standard Mean Ocean Water-Standard Light Antarctic Precipitation (VSMOW-SLAP) scale. ~~To ensure data quality, selected samples were analyzed in both laboratories, and the results were highly consistent, confirming the reliability of the measurements.~~

2.4 Data analysis

2.4.1 Estimation of mean transit time and mean residence time

The mean residence time (MRT) represents an effective, isotope-based measure of the average time that water resides within a given compartment before being transferred to downstream compartments. Rather than describing a precise physical storage duration, MRT characterizes the seasonally integrated effects of storage, mixing, and transport processes. In karst environments, where flow pathways are highly heterogeneous, MRT is particularly useful for describing the dominant seasonal storage behavior of water within soil, fracture, and rock compartments. For example, soil water at 50 cm depth may retain infiltrated rainfall for a certain period before contributing to deeper flow or evapotranspiration.~~The mean residence time (MRT) represents the average time during which water remains in a particular compartment before moving out. For example, 50 cm of soil may retain infiltrated rainfall for a certain period before it contributes to deeper flow or evaporation.~~ We estimated MRT using the amplitude damping approach (Małoszewski and Zuber, 1982; Reddy et al., 2006; Stewart and McDonnell, 1991; McGuire et al., 2002)~~.~~ , which interprets the attenuation of seasonal isotope signal amplitudes as a response to mixing and storage along flow pathways. This approach assumes that seasonal isotope variability provides an integrated signal of water storage and turnover at the timescale of interest, which is well suited for investigating seasonal water storage dynamics in karst systems.~~Amplitude damping reflects the attenuation of isotopic signal fluctuations due to processes such as dilution~~

~~and mixing during water transport.~~

The isotope sine curve analysis is used to estimate MRT by fitting a sinusoidal function to the isotope data of each compartment. We used the sine function fitting:

$$\delta^{18}O \text{ or } \delta D = a_1 cos(2\pi t) + a_2 \sin(2\pi t) + offset \quad (1)$$

Where , a_1 and a_2 are the amplitude parameters, and *offset* represents the baseline value.

We applied a sine function transformation to the isotopic time series ($\delta^{18}O$ or δD) as follows:

$$\delta^{18}O \text{ or } \delta D = A \cdot \sin(2\pi t - \phi) + offset \quad (2)$$

Amplitude (A) and phase (ϕ) were calculated as:

$$A = \sqrt{a_1^2 + a_2^2} \quad (3)$$

$$\phi = -atan2(a_1, a_2) \quad (4)$$

The MRT (in days) was calculated by:

$$MRT = c^{-1}\sqrt{f^{-2} - 1} \quad (5)$$

$$f = \frac{A_n}{A_m} \quad (6)$$

Where A_n and A_m are the amplitudes of the output and input isotope signals, respectively. The damping factor (f) was used to describe how the amplitude of the isotope signal is reduced as it moves through different compartments.

The isotope time series used for the estimation of MTT and MRT spans the entire period from September 2022 to March 2025 and therefore includes data analyzed in both laboratories. As shown by the precipitation isotope record (Fig. 2) and the isotopic dynamics of soil water, rock water, and xylem water (Figs. B1–B3), the isotope signals over this period exhibit smooth and continuous seasonal variations with clear sinusoidal characteristics. No discontinuities or step changes are observed at the transition between the two analytical phases, indicating good continuity and consistency between datasets obtained from the two laboratories. This temporal coherence results in stable sinusoidal fitting and low uncertainties in the estimation of MTT and MRT.

带格式的: 缩进: 首行缩进: 2 字符

2.4.2 MixSIAR model

To analyze the partitioning of water sources among plants in our karst ecosystem, we employed the MixSIAR Bayesian Mixing Model (BMM). By integrating isotopic data, we gained a comprehensive understanding of the contributions of various water sources to plant water uptake. MixSIAR is a stable isotope analysis package in R that estimates water source contributions through a Bayesian approach, using Markov Chain Monte Carlo (MCMC) methods to generate posterior distributions of source proportions. The MCMC algorithm runs on multiple chains to ensure convergence and reliable posterior estimates (Moore and Semmens, 2008; Stock and Semmens, 2016; Parnell et al., 2013). One of the main advantages of MixSIAR over traditional mass balance methods is its reduced sensitivity to isotopic fractionation effects (Evaristo et al., 2017), and it incorporates uncertainties from the sources by introducing prior information, multiple continuous covariates, and error structures to improve prediction accuracy (Gai et al., 2023; Liu et al., 2024a). This robustness is particularly well-suited to karst ecosystems, where the isotopic composition of water sources can vary significantly due to complex interactions among

soil, rock fractures, and vegetation (Gai et al., 2023).

The quantitative water source partitioning using the MixSIAR model is based exclusively on samples collected from April 2024 to March 2025. All samples used for source partitioning were processed and analyzed at the University of Saskatchewan, Canada. This analytical design minimizes potential inter-laboratory variability and ensures internal consistency among water sources, particularly for bulk soil water, which was extracted and analyzed only in Canada.

2.4.3 Calculation Method of Evaporation Index

The evaporation degree of different water bodies relative to local precipitation is characterized using the linear offset (Lc-excess) from the Local Meteoric Water Line (LMWL), as proposed by Landwehr and Coplen (2006):

$$Lc - excess = \delta D - a \times \delta^{18}O - b \quad (7)$$

where a and b are the slope and intercept of the LMWL, respectively.

3. Results

3.1 Temporal variation in isotope values and water conditions within water pools

~~Fig. 2 shows that the $\delta^{18}O$ and δD values of precipitation exhibit periodic sinusoidal fluctuations with the seasons, closely related to changes in precipitation amount and temperature. During the summer and autumn months (June to September), when rainfall is more abundant, the precipitation primarily originates from maritime air masses, with noticeably more negative $\delta^{18}O$ and δD values, indicating the influence of the amount effect. Moreover, after intense rainfall events, $\delta^{18}O$ and δD values decrease sharply in a short period, reflecting the significant impact of intense rainfall on the local hydrological cycle, suggesting that such precipitation may originate from the input of atmospheric water vapor from higher altitudes. During the winter and spring months (December to April), precipitation is mainly controlled by continental air masses, with relatively higher $\delta^{18}O$ and δD values, reflecting isotopic enrichment characteristics caused by lower rainfall amounts and stronger evaporation effects.~~

The isotopic signatures of different water pools within the karst critical zone exhibited clear spatial and temporal variability, reflecting the contrast between dynamic precipitation inputs and more buffered subsurface reservoirs.

As shown in Fig. 2, the $\delta^{18}O$ and δD values of precipitation displayed pronounced seasonal fluctuations that followed changes in precipitation amount, temperature, and moisture source. During summer and early autumn (June–September), abundant rainfall associated with maritime air masses resulted in relatively depleted isotopic values. After major rainfall events, isotope values decreased rapidly. This depletion is consistent with the combined influence of the amount effect, convective mixing, reduced sub-cloud evaporation, and shifts in moisture source regions. In contrast, precipitation during winter and spring (December–April) was mainly influenced by continental air masses and lower precipitation amounts, resulting in comparatively enriched $\delta^{18}O$ and δD values.

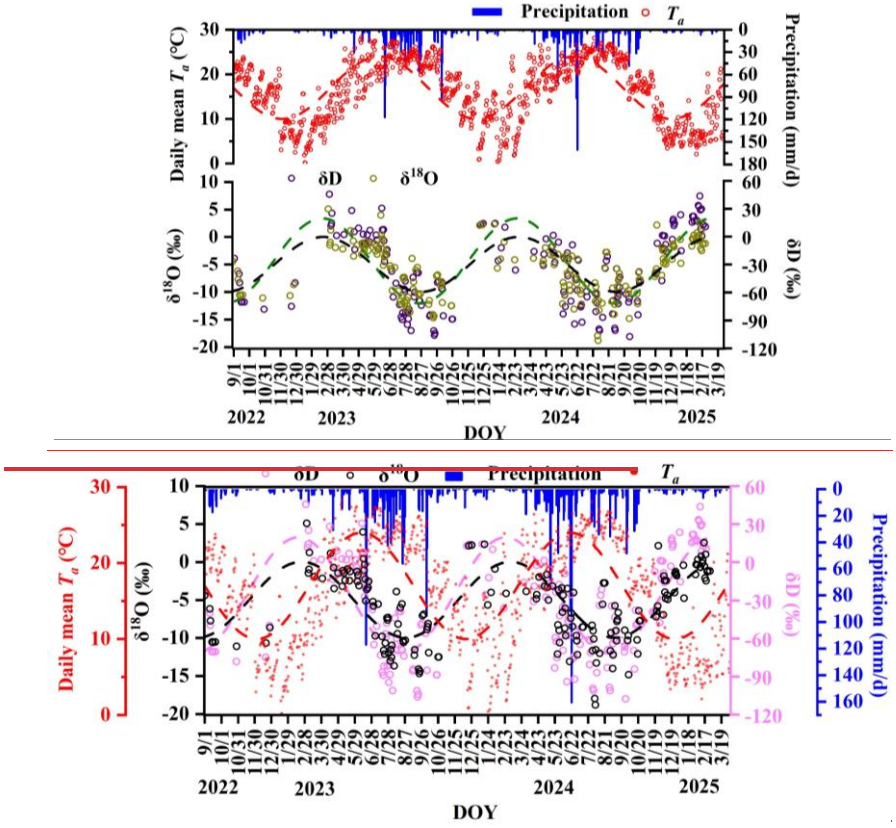

Figure 2. Temporal variations in stable isotopes of precipitation (δD and $\delta^{18}O$), rainfall amount, and daily average temperature.

The arithmetic mean values of precipitation (mean $\delta^{18}O = -6.00‰$, $\delta D = -35.66‰$) were used to represent the central tendency of the seasonal signal. The Local Meteoric Water Line (LMWL: $\delta D = 8\delta^{18}O + 9.93$) closely overlapped with the Global Meteoric Water Line (Fig. 3), suggesting that precipitation isotopes in the study region are primarily controlled by moisture source rather than significant evaporative fractionation during atmospheric transport.

After infiltration, the isotopic compositions of subsurface water pools diverged from those of precipitation due to the structural heterogeneity of the soil-rock system. Mobile soil water (mean $\delta^{18}O = -6.57‰$, $\delta D = -43.79‰$) exhibited a relatively wide isotopic range and clear seasonal fluctuations that broadly followed the precipitation signal (Figs. B1a, B1b). These

variations likely reflect the combined effects of depleted rainfall inputs during the wet season, evaporative enrichment during dry periods, and rapid mixing within the shallow soil profile. In contrast, bulk soil water showed more depleted mean isotopic values (mean $\delta^{18}O = -8.13‰$, $\delta D = -59.61‰$) and a more damped temporal signal. While shallow bulk soil water (0–30 cm) displayed noticeable fluctuations associated with evaporation and recent rainfall inputs, deeper soil water (>30 cm) remained relatively stable in both isotopic composition and moisture content (Fig. B1c), indicating slower water turnover and stronger mixing of older water.

Hydrological behavior at the soil-rock interface differed from that of the surrounding soil matrix. Soil-rock interface water (mean $\delta^{18}O = -6.77‰$, $\delta D = -46.69‰$) responded more rapidly to rainfall events and showed larger moisture fluctuations than adjacent soil water (Fig. B1d). This pattern indicates that the interface likely functions as a preferential flow zone rather than a slowly percolating matrix domain.

The isotopic variability of rock fracture water also depended on fracture characteristics. Rock fracture water (mean $\delta^{18}O = -6.89‰$) and infilled rock fracture water (mean $\delta^{18}O = -6.73‰$) exhibited different temporal stability depending on fracture aperture and the presence of soil infill (Fig. B2a and Fig. B2b). Shallow and narrow fractures (e.g., 45–60 cm at site B) showed relatively large fluctuations, suggesting rapid recharge from recent rainfall. In contrast, deeper fractures (e.g., 244–306 cm at site C) and large fractures filled with soil (e.g., 10–21 mm at site B and 38 mm at site C) exhibited more stable isotopic signals and weaker moisture fluctuations (Fig. B2c). These observations suggest that soil infill can reduce rapid infiltration and enhance water retention within fractures, allowing them to function as relatively stable subsurface water reservoirs.

Plant xylem water isotopes (overall mean $\delta^{18}O = -5.99‰$, $\delta D = -51.12‰$) reflected the integration of these different subsurface water pools. Xylem water samples plotted below the LMWL and aligned along a soil water line with a slope of approximately 6 (Fig. 3). This offset likely reflects isotope fractionation associated with soil evaporation and the mixing of different source waters within the soil-rock system. Seasonal variations in xylem isotopes broadly followed the availability of different water sources (Figs. B3a and B3b) but also exhibited clear spatial differences among sites. For example, trees at site B showed relatively enriched isotopic values (mean $\delta^{18}O = -5.50‰$, $\delta D = -49.58‰$), consistent with the isotopic composition of local water sources. In contrast, trees at sites A and C&D showed more depleted xylem isotopic signatures (mean $\delta^{18}O = -6.04‰$ and $-6.17‰$, respectively). These spatial differences suggest that vegetation water uptake is strongly influenced by local hydrological conditions, including soil water availability, root distribution, and access to different subsurface water pools.

~~Fig. 3 indicates that the average $\delta^{18}O$ value of rainfall in the study area is -6‰, and the average δD value is -35.66‰, with a wide range of variations. It presents the LMWL for the study area, with a slope of 8 and an intercept of 9.93, which is consistent with the Global Meteoric Water Line (GMWL), indicating that the precipitation isotopes in the study area are mainly controlled by the source of precipitation and the amount effect, without significant non-equilibrium evaporation during atmospheric transport.~~

~~Fig. 3 indicates that there are significant differences in the $\delta^{18}O$ and δD values of mobile soil water and bulk soil water~~

across various sampling sites in the study area. The average $\delta^{18}O$ for mobile soil water is -6.57‰, with average δD is -43.79‰, showing a broad overall range ($\delta^{18}O$: -16.99 to 1.27‰; δD: -127.87 to 5.89‰). Appendix Figs. A1a and A1b depict the distinct sinusoidal fluctuations in $\delta^{18}O$ and δD for mobile soil water, which become enriched after the reduction in precipitation in September and shift towards more negative values following increased precipitation in April, aligning with the isotopic characteristics of precipitation.

In contrast, bulk soil water exhibits lower isotopic values, with average $\delta^{18}O$ is -8.13‰ and average δD is between -59.61‰. Fig. 3 shows that the overall evaporation line slope of bulk soil water (8.21) aligns with the precipitation line and is higher than that of mobile soil water (7.53). The isotopic trends of bulk soil water also show sinusoidal fluctuations, with shallow soil water (0-30 cm) affected more significantly by precipitation and evaporation, showing more pronounced fluctuations, while deeper soil water (> 30 cm) changes more gradually. Additionally, Appendix Fig. A1c shows that shallow soil moisture content fluctuates significantly, especially at the surface 5 cm, while deeper soil moisture remains relatively stable. Soil moisture content is highest at depths of 20-50 cm and lowest below 50 cm.

Soil-rock interface water have lower averages ($\delta^{18}O$ = -6.77‰, δD = -46.69‰) than mobile soil water but higher than bulk soil water. Appendix Fig. A1d shows that soil-rock interface moisture content responds more rapidly and with greater fluctuation to rainfall than the soil at the same depth, indicating that the soil-rock interface is not fully continuous but has preferential flow pathways, acting as rapid water transmission channels during rainfall infiltration, thus aligning its hydrological dynamics more closely with rock fracture water rather than the slow response patterns of surrounding soil water.

The mean $\delta^{18}O$ and δD values of rock fracture water were -6.89‰ and -44.39‰, respectively, while those of infilled rock fracture water were -6.73‰ and -46.11‰. However, the overall evaporation line slope for rock fracture water (8.31) was greater than that of infilled rock fracture water (6.76). Appendix Figs. A2 further reveal isotopic and moisture characteristics of rock fracture water under different fracture apertures and depths. For instance, at site B, shallow fracture water (45-60 cm) $\delta^{18}O$ and δD values (Figs. A2a and b) and moisture content (Fig. A2c) fluctuate significantly, indicating primary influence by short-term rainfall, whereas at site C, deep fracture water (244-306 cm, narrower aperture 0.16-0.26 mm) shows smaller fluctuations in $\delta^{18}O$, δD, and moisture content, indicating slower water renewal rates. In larger fractures filled with soil, such as at sites B (10-21 mm) and C (38 mm), the isotopic values and moisture content of fracture water show smaller fluctuations compared to adjacent depths, suggesting that soil filling reduces the impact of rapid infiltration from rainfall, making the water replenishment process more stable.

The mean $\delta^{18}O$ and δD values of xylem water were -5.99‰ and -51.12‰, respectively. The relatively depleted δD and the overall evaporation line slope of 6 suggest a deviation below the LMWL, indicating stronger evaporative enrichment.

Appendix Figs. A3a and A3b show that the $\delta^{18}O$ and δD values of xylem water in trees exhibit seasonal fluctuations similar to those of the water sources, and the $\delta^{18}O$ and δD values of various water sources at different sites show certain similarities, directly influencing the isotopic characteristics of tree xylem water. For example, water sources at site B are overall more enriched, while those at sites A and C&D are more depleted, leading to more enriched isotopic values in xylem water at site B (average $\delta^{18}O$ -5.50‰, average δD -49.58‰) compared to site A ($\delta^{18}O$ -6.04‰, δD -51.57‰) and sites C&D ($\delta^{18}O$ -

~~6.17‰, δD -51.90‰). This difference indicates that the water use by vegetation is directly controlled by the hydrological conditions at different sites.~~

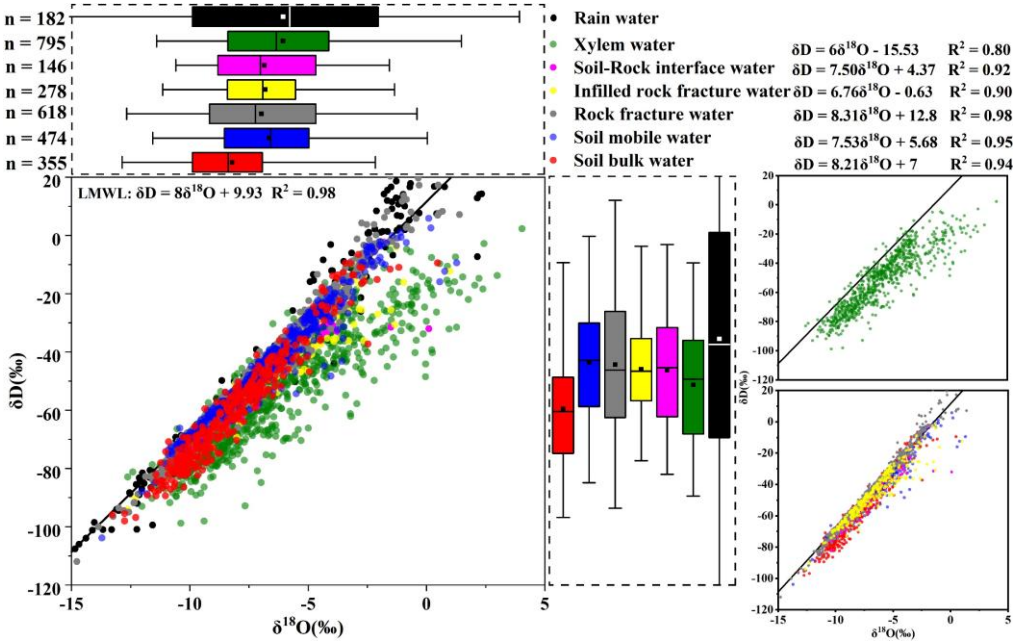

Figure 3. δD-δ^{18}O relationship diagram for different water bodies during various periods.

3.2 Factors affecting MRT in different water pools

~~Appendix Table B1 lists the MRT for mobile soil water and bulk soil water at different sample sites and soil depths. The MRT of soil water at different sites are influenced by a combination of soil depth and permeability, showing distinct spatial distribution characteristics. Overall, soil water MRT ranged from 36 to 708 days, with an average of 177 days. Specifically, the MRT of bulk soil water (36–708 days, mean 196 days) was higher than that of mobile soil water (63–459 days, mean 143 days). Similarly, by referencing tree root depths from Table B4 and the corresponding soil water MRTs from Table B1, we found that bulk soil water within the root zone (36–177 days, mean 95 days) exhibited a longer residence time than mobile soil water (63–144 days, mean 88 days).~~

~~The MRT at site B (49–708 days, mean 365 days) was significantly higher than that at other sites (36–144 days, mean 88 days), indicating substantial differences in water retention characteristics among water types and sampling locations. With increasing soil depth, MRT of bulk soil water increased markedly. For example, at site B, MRT ranged from 49 to 177 days~~

~~(mean 123 days) at depths of 5-20 cm. When depth exceeded 50 cm, MRT increased to 244-708 days (mean 513 days), suggesting that deep soil water has significantly longer residence times and lower transport rates. In contrast, the MRT of mobile soil water gradually decreased with depth from 50 to 180 cm. This suggests that deep mobile water may be replenished by preferential flow along soil-rock interfaces or fractures. The opposing depth-dependent MRT patterns between mobile and bulk soil water indicate their different hydrological functions. Bulk soil water serves as a stable storage with slow turnover, whereas mobile soil water, functions as a transient reservoir connected to rapid flow paths such as fractures.~~

~~Soil K_h also played a crucial role in controlling MRT. As shown in Fig. 4, MRT of bulk soil water decreased exponentially with increasing K_h. When K_h exceeded 0.75 cm·h^{-1}, MRT stabilized around 110 days. In deep soils (> 50 cm) at site B, K_h values ranged only from 0.1 to 0.18 cm·h^{-1}, substantially lower than those at other sites (0.75-2.33 cm·h^{-1}) which severely restricted water movement and resulted in significantly elevated MRT values. This indicates that in low-permeability soils, water has a longer residence time and slower renewal rate, whereas in high-permeability soils, water is replenished more rapidly, resulting in shorter MRT.~~

The residence times of soil water and soil-rock interface water were fundamentally controlled by permeability and depth, reflecting a clear divergence between stable storage and rapid preferential flow paths. Overall, bulk soil water exhibited significantly longer residence times (mean MRT = 196 days) than mobile soil water (mean MRT = 135 days) (Table C1). This divergence was strongly regulated by soil hydraulic conductivity (K_h). As shown in Fig. 4, the MRT of bulk soil water decreased exponentially with increasing K_h, stabilizing when K_h exceeded 0.75 cm·h^{-1}. In deep, low-permeability soils (e.g., >50 cm at site B, where K_h ranges only from 0.1 to 0.18 cm·h^{-1}, bulk water MRT extended up to 708 days (mean 513 days)), functioning as a slow-turnover storage pool. Conversely, the water at the soil-rock interface renewed rapidly (mean 118 days compared to 513 days for adjacent bulk soil; Table C2). These contrasting patterns demonstrate that while the soil matrix retains water long-term, deep mobile water is rapidly replenished via preferential flow along soil-rock interfaces.

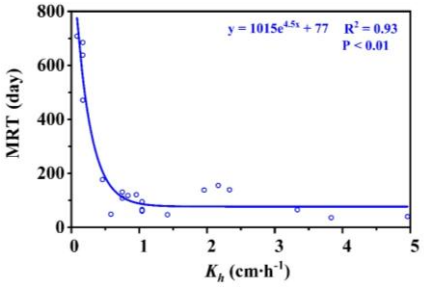

Figure 4. Relationship between K_h and MRT of bulk soil water.

~~Table B2 shows that at site B, the MRT of soil-rock interface water (21-214 days, mean 118 days) were significantly lower than that of soil water at the same depth (244-708 days, mean 513 days; see Table B2). These results indicate that the~~

~~soil-rock interface has higher permeability and more developed preferential flow pathways, leading to a faster renewal rate of water at the interface. Consequently, soil-rock interface water is more responsive to precipitation inputs but has lower retention capacity.~~

~~Table B3 presents the MRT of rock fracture water under different fracture apertures and burial depths. Overall, MRT ranged from 23 to 303 days (mean 117 days), showing pronounced spatial heterogeneity influenced by fracture aperture, depth, and recharge conditions. For shallow fractures (burial depth 45-80 cm, aperture 0.47-2 mm), MRT ranged from 23 to 91 days, indicating that shallow fracture water is strongly influenced by precipitation and has a high renewal rate. At site A, deep fractures (270-600 cm) exhibited MRTs of 108-182 days, while fractures at sites C&D (244-306 cm depth) showed MRTs of 118-124 days. This suggests that deep fracture water is primarily recharged by old water, resulting in slower renewal and a more damped isotopic signal. A significant relationship was observed between MRT and fracture aperture (Fig. 5). Notably, when fracture width exceeded 10 mm, MRT increased substantially with aperture size, ranging from 84 to 303 days (mean 172 days). This is primarily due to the presence of soil infill in large fractures (porosity 0.41–0.74), which enhances the water-holding capacity and prolongs water retention time. This process has important implications for plant water use: infilled rock fractures can provide a more stable water supply under drought conditions, thereby increasing water availability and potentially influencing the water uptake strategies of different plant root systems.~~

Crucially, the retention capacity of bedrock water was directly dictated by fracture architectural traits, specifically aperture size and the presence of soil infill (Fig. 5). While shallow, narrow fractures (aperture 0.47–2 mm, depth 45–80 cm) exhibited rapid renewal driven by precipitation (MRTs of 23–91 days), deeper and wider fractures showed pronounced storage capabilities (Table C3). A significant positive threshold relationship emerged: when fracture aperture exceeded 10 mm (Fig. 5), MRT increased substantially, ranging from 84 to 303 days (mean 172 days). This extended retention is primarily driven by soil infill within these larger fractures (porosity 0.41–0.74), which fundamentally transforms fractures from rapid downward conduits into highly retentive subsurface reservoirs. This structure-dependent storage mechanism provides a critical ecohydrological buffer, enabling infilled fractures to maintain a stable water supply under drought conditions (Hasenmueller et al., 2017; Zhang et al., 2016; Carrière et al., 2019; Yan et al., 2023; Howarth and Bishop, 2023).

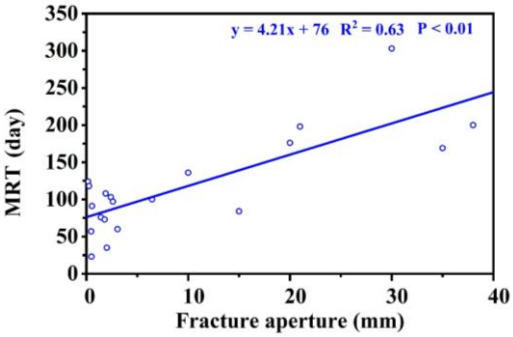

Figure 5. Relationship between aperture and MRT of rock water.

The distinct residence times of these environmental water pools directly shaped the water uptake strategies of different trees, as reflected in the MRT of their xylem water. (Note: xylem MRT characterizes the mixing volume and turnover time within the tree-source system, whereas MTT quantifies the transit lag time from source to xylem; Table C4). At site A, trees exhibited similar MRTs across all water sources (31–64 days), indicating a highly flexible, opportunistic strategy utilizing both transient mobile water and moderately retained rock water. In contrast, at sites with well-developed infilled fractures (Sites B and C&D) or thick retentive soils (Site E), trees demonstrated a targeted reliance on long-residence water to support sustained transpiration. For instance, the large tree ts_6 at site C dynamically tapped into long-residence rock and bulk water (xylem MRT up to 124–128 days) to support its exceptionally high transpiration demand (average sap flow rate of 1.3 $cm \cdot h^{-1}$). Similarly, evergreen trees ($cc_{1\text{-}3}$) consistently utilized long-MRT bulk and rock water (73–76 days) to maintain year-round physiological activity compared to deciduous species. Furthermore, the interplay between soil retention and fracture traits dictates site-specific resilience. At site E, where rock fractures are poorly developed (apertures < 2.6 mm) but soils possess high water-holding capacity (higher soil moisture content, Fig. B1c), the xylem MRT associated with bulk soil water (72–88 days) was notably longer than that of the limited rock water (51–61 days). This demonstrates that in the absence of large infilled fractures, the retentive soil matrix serves as the more stable and persistent moisture pool. Collectively, these xylem MRTs confirm that trees systematically align their root uptake with the specific geological compartments—either retentive soil matrix or infilled rock fractures—that offer the most stable, long-residence water supply.

~~Table B4 details the MRT for different water sources in various trees, reflecting the time it takes for mobile soil water, bulk soil water, and rock water to be absorbed from the rhizosphere to the tree interior, as well as the duration these water sources stay within the trees.~~

~~There are significant differences in the MRT of different water sources within the trees at different sites, indicating spatial heterogeneity in plant water use strategies. At site A, the differences in MRT among the three water sources are relatively minor (MRT_1 ranges from 39 to 59 days, MRT_2 from 44 to 64 days, MRT_3 from 31 to 53 days), suggesting that trees at this~~

带格式的: 缩进: 首行缩进: 2 字符

~~site have a flexible water use strategy. They can simultaneously utilize mobile soil water, bulk water, and rock fracture water to adapt to spatial and temporal variations in water supply. In contrast, at site B (MRT_1 ranges from 14 to 40 days, MRT_2 from 38 to 94 days, MRT_3 from 79 to 100 days), sites C&D (MRT_1 from 8 to 96 days, MRT_2 from 32 to 124 days, MRT_3 from 25 to 128 days), and site E (MRT_1 from 13 to 32 days, MRT_2 from 72 to 88 days, MRT_3 from 51 to 61 days) show more pronounced differences in water source utilization. Bulk water and rock water have longer retention times, while mobile water has the shortest retention time, averaging only 44% and 48% of the retention times of bulk water and rock water, respectively. This suggests that at these sites, vegetation relies more on water sources with longer retention times, while the proportion of mobile soil water, which replenishes quickly, is relatively low, possibly serving primarily to supplement short-term high transpiration demands.~~

~~Additionally, the xylem water of trees at site ts_6 shows retention times for bulk water and rock water up to 124–128 days, and mobile water up to 96 days, indicating ts_6's capability to utilize long-standing water sources combined with short-term available water to support its high transpiration demand (average sap flow rate of 1.3 $cm \cdot h^{-1}$). This strategy maintains its high water consumption.~~

~~Evergreen trees at sites $cc_{1,3}$ also show long retention times for bulk water and rock water (73–76 days) compared to deciduous trees, suggesting that evergreens rely more on a stable deep water supply to maintain physiological activities throughout the year.~~

~~Moreover, trees at site E primarily rely on bulk soil water, as indicated by its longer retention time (72–88 days) compared to mobile water (13–32 days) and rock water (51–61 days), suggesting that the site's soil has strong water-holding capacity (illustrated in Figure A1c, higher SMC), providing a relatively stable water supply to the trees.~~

3.3 Partitioning of plant water sources

Derived from the MixSIAR model outputs, Figs. 6 and Fig. D1 illustrate the proportional use of four water sources (bulk soil water, mobile soil water, rock fracture water, and infilled rock fracture water) across six phenological and hydrological periods (from senescence in October–November to late growing season in August–September). Our results reveal a clear structure-dependent water uptake strategy, where the importance of rock water is strongly governed by fracture traits and seasonal water availability, rather than uniform temporal shifts.

During periods of abundant water supply, the influence of fracture properties on water sourcing was minimal. In the peak growing season (June–July; Fig. 6 and Fig. D1e), the contribution of mobile soil water increased markedly across all sites (mean 41%), especially at sites A (mean 53%) and C&D (mean 47%). At sites C&D, the average contribution of infilled rock fracture water declined from 37% (April–May) to 15% (Fig. 6c), indicating that large fractures serve a regulatory storage function, storing excess water for later use, rather than acting as a dominant source during the rainy season.

Conversely, during dry and transitional periods (senescence, dormancy, reactivation, late and early growing season), tree water sourcing diverged significantly depending on local fracture aperture and infill conditions. At sites with highly developed and soil-filled fractures, trees demonstrated a strong capacity to exploit deep rock water to buffer drought. For instance, Table C3 shows that soil-filled fractures (>20 mm) at C&D have MRTs as long as 169–303 days (mean 212 days). These infilled

structures act as stable, long-residence water pools that persist across seasons. As temperatures rose during the reactivation period (February–March), trees at sites C&D expanded their reliance on rock water to a mean of 69% (Fig. 6c), with individual contributions ranging from 47% to 88% (Fig. D1c), supporting budburst before substantial rainfall resumed. This structural dependence persisted into the early growing season (April–May) and scaled with tree root-zone fracture volume. The largest tree (ts_6, DBH 36 cm; Table A3), whose root zone contained the highest fracture volume (2.19 m^3, of which 87–96% was soil-filled), derived up to 85% of its water from rock sources, including 74% from infilled rock fracture water (Fig. D1d). Additionally, Table C4 indicates that ts_6 uses rock water with a residence time of up to 128 days, demonstrating its capacity to access stable, long-residence water for transpiration. Collectively, these findings confirm that large, infilled rock fractures function as critical "transitional reservoirs", alleviating early-season soil water deficits.

This fracture-dependent buffering effect was also evident during the late-season dry-down. As rainfall and soil moisture declined in the late growing season and senescence periods, the availability of recent precipitation diminished. Trees at site B continued to rely heavily on infilled rock fracture water in senescence period (mean 49% in Fig. 6b). Similarly, trees at site A ($bp_{1\text{-}3}$) showed a substantial increase in rock fracture water use, jumping from mean 10% in late growing season to mean 44% in senescence period (Fig. 6a). Because large fractures maintain higher moisture content than rapidly depleting shallow soils (Fig. B2c vs. Fig. B1c), rock water provides an essential supplementary source preventing severe water stress during the wet-to-dry transition.

In stark contrast, trees at sites lacking large, infilled fractures exhibited entirely different survival strategies. Site E exhibited the least developed rock fractures (aperture <2.6 mm; Table C3). Throughout most of the year, including critical dry periods, these trees' reliance on rock water remained below 30%. Without the deep buffering capacity of infilled fractures, these trees were forced to depend heavily on soil water. During the early growing season, individuals at site E relied on soil water for 82–91% in Fig. D1d (mean 88% in Fig. 6d) of their uptake. Even during the dormancy period (December–January), these rock-water-limited environments relied on minor rainfall pulses to recharge near-surface soil water (mean 67% in Fig. 6d). However, due to the low rock permeability at this site (K_b < 47 cm·h^{-1}; Table C3), water loss through deep percolation was limited. As a result, the average soil moisture content was relatively stable (Fig. B1c), enabling this soil-dependent strategy despite the absence of usable rock water.

~~Based on the MixSIAR model outputs, Figs. 6a–f illustrate the proportional use of four water sources: bulk soil water, mobile soil water, rock fracture water and infilled rock fracture water by trees at different sites across various months~~

~~During the late growing season (October–November; Fig. 6f), which marks the transition from wet to dry conditions, the proportion of bulk water used by trees generally increases (14–80%, mean 55%). As rainfall decreases significantly after October (Fig. 2) and soil moisture declines (Fig. A1c), the availability of recent precipitation diminishes, leading trees to rely more on long-residence bulk water to meet minimal physiological demands.~~

~~During the cold and dry winter months (December–January), monthly precipitation was less than 25 mm, and tree sap flow density declined to its annual minimum, indicating limited water use by tree. As shown in Fig. 6a, however, trees still exhibited relatively high uptake of mobile soil water (30–54%, mean 39%). Previous studies have shown that even small~~

precipitation events can temporarily elevate soil moisture content (SMC > 0.2), thereby stimulating transpiration in trees (Liu et al., 2025). This suggests that minor rainfall pulses during the dry season may be sufficient to recharge mobile water in near-surface soils, which, despite their transient nature, can still meet short-term water demands of shallow-rooted plants or maintain baseline physiological functions in trees. In addition, at sites C&D, which have abundant rock water sources (including rock fracture water and infilled rock fracture water), trees derived 40–44% (mean 42%) of their water from these sources during the winter months.

As temperatures began to rise in February and March (early spring), tree water use also increased. During this period, trees at sites C&D further expanded their reliance on rock water, with contributions reaching 47–88% (mean 69%) in Fig. 6b. In contrast, trees at other sites with limited rock water availability showed increased uptake of mobile soil water (43–72%, mean 57%), reflecting a greater dependence on short-term rainfall inputs. February to March represents a critical period for budburst and root activity in many tree species. These contrasting patterns suggest that in areas with well-developed rock fractures and soil-filled fractures, trees can draw upon subsurface water reserves to meet early-season water demands before substantial rainfall resumes. Conversely, in rock water-limited environments, vegetation relies more heavily on episodic rainfall recharge of shallow mobile water to support transpiration recovery and physiological reactivation following the winter dormant period.

During the subsequent early growing season (April–May; Fig. 6c), substantial variation in water source use is observed among sites. Trees at sites A and E rely heavily on soil water (bulk and mobile), accounting for 63–91% (mean 77%) of uptake. In contrast, trees at sites C&D show the highest dependence on infilled rock fracture water (15–74%, mean 37%). The largest tree (ts_6, DBH is 36 cm in Table 4) derived up to 85% of its water from rock sources, including 74% from infilled rock fracture water. This is consistent with its root zone containing the highest fracture volume among all sampled trees (2.19 m^3 in Table 4) of which 87–96% volume is contributed by soil-filled fractures. Table 3 shows that soil-filled fractures (≥20 mm) at C&D have MRTs as long as 169–303 days (mean 212 days), enabling the storage of summer rainfall for gradual release into the following spring, thereby mitigating early-season soil water deficits. Additionally, Table 4 indicates that ts_6 uses fracture water with a residence time of up to 128 days, confirming its ability to extract long-residence water for growth and transpiration. As a large tree with an extensive and deep root system, ts_6 efficiently exploits deep fracture water. In contrast, smaller individuals at site E (bp_5, kp_{1_2}) receive lower contributions from rock water (9–12%), relying more on shallow soil water (< 50 cm depth). These findings suggest that long-residence rock fracture water acts as a 'transitional reservoir', providing critical water to support tree budding and transpiration at the onset of the growing season.

During the peak rainy season (June–July; Fig. 6d), the contribution of mobile soil water increases markedly (20–68%, mean 41%), especially at sites C&D (33–68%, mean 47%) and A (49–59%, mean 53%). This shift indicates that rainfall-driven replenishment of mobile soil water becomes the primary water source for vegetation. At the same time, the average contribution of infilled rock fracture water at C&D declines from 37% (April–May) to 15%, suggesting that in the rainy season, fracture water plays a more regulatory role, storing excess water for later use, rather than serving as the dominant source.

In August–September (Fig. 6e), the reliance on bulk water at sites C&D increases significantly from 14–27% (mean 20%)

in June-July to 35-58% (mean 49%), while the use of mobile soil water drops to 10-20% (mean 16%). Combined with soil moisture data from Fig. A1c, which shows low SMC (< 0.2) in the 20-50 cm layer at C&D during this period, these trends suggest a decline in shallow soil water availability, prompting greater dependence on slowly released bulk water. In contrast, trees at site A (bp_{1-3}) increase their use of mobile water to 76-82% (mean 79%), supported by relatively high soil moisture (> 0.2) at 20-50 cm depth.

During the late growing season (October-November; Fig. 6f), which marks the transition from wet to dry conditions, the proportion of bulk water used by trees generally increases (14-80%, mean 55%). As rainfall decreases significantly after October (Fig. 2) and soil moisture declines (Fig. A1e), the availability of recent precipitation diminishes, leading trees to rely more on long-residence bulk water to meet minimal physiological demands.

Notably, trees ts_4 and ts_2 at site B continued to rely heavily on infilled rock fracture water during this period, with contributions of 39% and 58%, respectively. Similarly, trees at site A (bp_{1-3}) show a substantial increase in rock fracture water use: from 9-12% (mean 10%) in August-September to 43-44% in October to November. This change is consistent with the rapid depletion of soil water after the rainy season (Fig. A1e), whereas fracture water remains available due to higher fracture moisture content (Fig. A2c). Rock water thus provides an essential supplementary source during the transition from wet to dry season, sustaining tree water use after soil water exhaustion and preventing severe water stress.

In addition, site E exhibited the least developed rock fractures (aperture < 2.6 mm; Table B3). Throughout most of the year, the trees reliance on rock water remained below 30%. However, due to the low rock permeability at this site (K_s < 47 $cm \cdot h^{-1}$; Table B3), water loss through deep percolation was limited. As a result, the average soil moisture content was relatively high (0.204-0.298; Table B1), and trees primarily relied on soil water for transpiration.

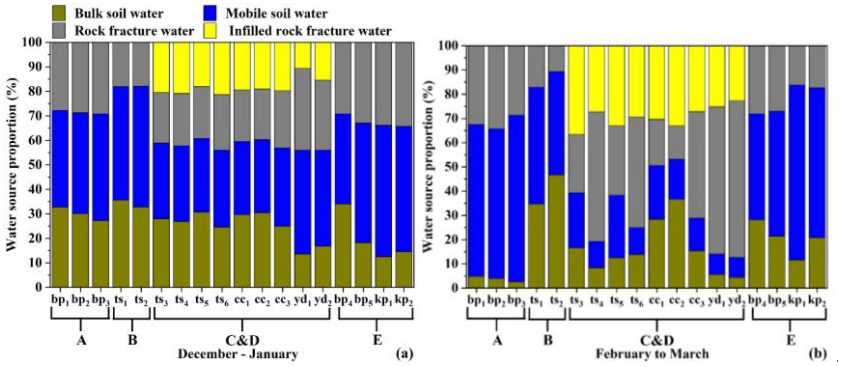

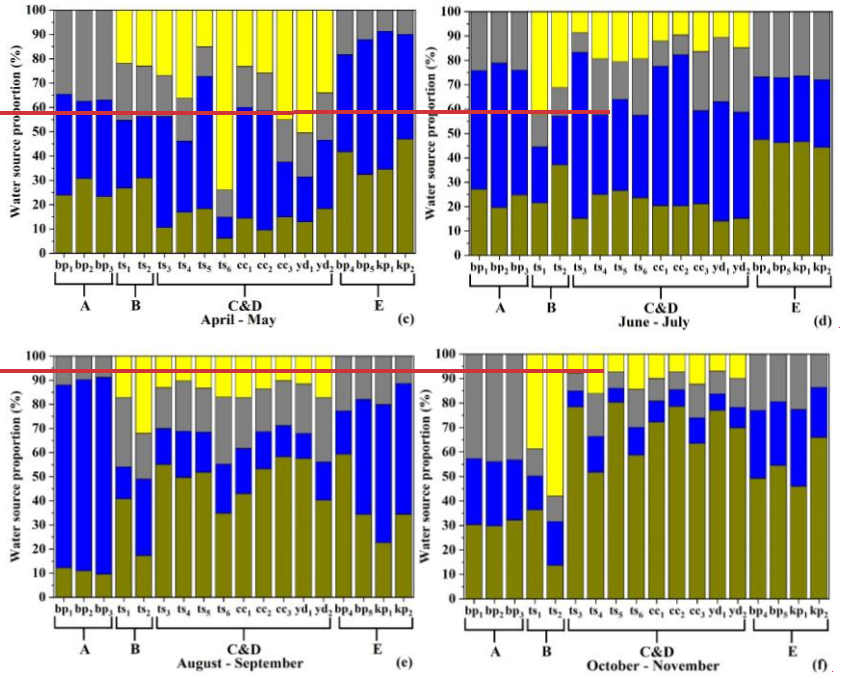
Water source proportion (%)
A
B
C&D
E
April - May
(c)
June - July
(d)
August - September
(e)
October - November
(f)

680

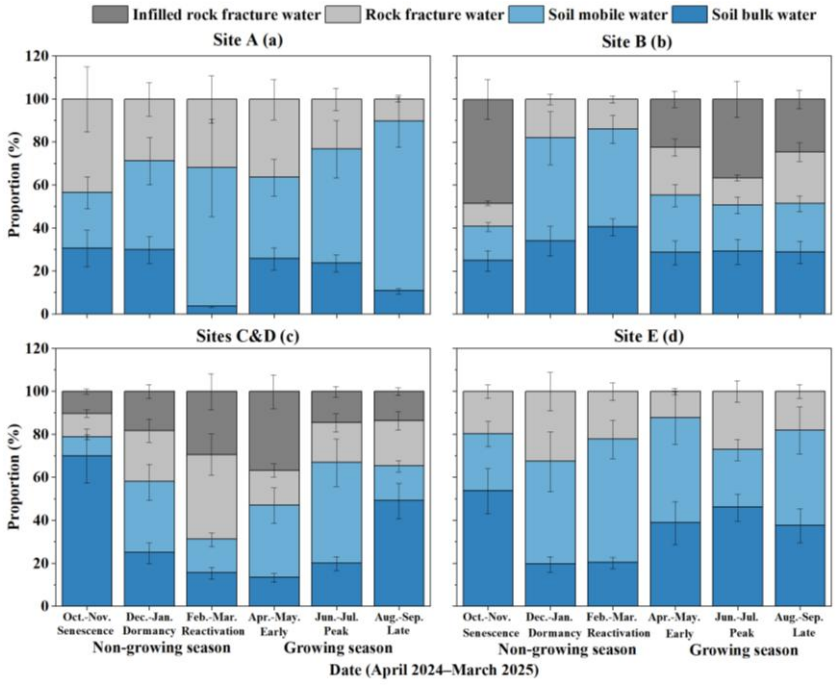

~~Figure 6. Partitioning of tree water sources by month.~~Figure 6. Seasonal variations in the mean proportional contribution of water sources to tree xylem water, grouped by fracture aperture and infill characteristics. Data were collected from April 2024 to March 2025. The panels represent the representative fracture type defining each micro-habitat (noting that while minor fractures are ubiquitous, soil-filled fractures dominate storage at Sites B – D): (a) Site A: medium open fractures (aperture 3 – 10 mm, no infill); (b) Site B: fully infilled fractures (aperture 10 – 20 mm, fully infilled); (c) Sites C&D: wide partially infilled fractures (aperture >20 mm, partially infilled); (d) Site E: narrow open fractures (aperture <3 mm, no infill).The X-axis displays data in 2-month intervals corresponding to distinct plant phenological stages (e.g., growing season (early growing, peak growing, late growing), senescence, reactivation, dormancy). Data represent the mean values of all sampled trees within each site group, Error bars indicate ±1 standard deviation (SD) derived from the MixSIAR model outputs.

4. Discussion

4.1 Rock fracture properties drive isotopic variability and ecohydrological responses of vegetation

~~This study provides a mechanistic assessment of the role of rock fractures on plant water uptake of rock moisture. Our work shows how fracture water can serve as a deep and temporally buffered reservoir, supporting plant water needs during transitional periods. During both the pre-growing season and early growing season (February-May), rock water plays a critical role in reactivating deciduous tree growth. During the peak rainy season (June-July), rainfall-driven mobile soil water~~

带格式的: 两端对齐
设置了格式: 字体: 9 磅, 加粗
设置了格式: 字体: 9 磅
设置了格式: 字体: 9 磅, 加粗
设置了格式: 字体: 9 磅
设置了格式: 字体: 9 磅, 加粗
设置了格式: 字体: (默认) Times New Roman

~~dominates plant uptake, rapidly recharging the root zone to support high transpiration. As precipitation declines in late summer (August onward), trees increasingly rely on bulk soil water and rock water to meet their physiological demands through the dry season.~~

Our findings provide a critical karst-specific extension to the classic 'ecohydrological separation' hypothesis. Traditionally, this concept posits that trees primarily utilize tightly bound soil water, while mobile water bypasses the root zone ~~This flexible adaptation enables vegetation to cope with seasonally dynamic and structurally complex hydrological conditions. These results in some ways support the notion of ecohydrological separation~~ (McDonnell, 2014; Evaristo et al., 2015; Brooks et al., 2010)~~.~~. Conventional studies attribute this separation primarily to soil-specific factors, such as low soil water content, preferential flow paths, and coarse-textured, low-saturation soils with poor hydraulic conductivity~~Conditions such as low soil water content, preferential flow paths, and coarse-textured soils reinforce this separation~~ (Finkenbiner et al., 2022; Liu et al., 2020; Finkenbiner et al., 2021; Sprenger et al., 2016). However, in karst landscapes characterized by extremely shallow soils, the soil matrix alone is insufficient to sustain year-round transpiration (Liu et al., 2025). Our results demonstrate that this functional separation is not confined to the soil but extends deep into the epikarst architecture. Crucially, the structural complexity of the karst subsurface — specifically variations in fracture aperture and the degree of soil infill — creates a massive, compartmentalized reservoir of 'bound' water, limiting mixing among water pools and reinforcing their functional separation.~~The structural complexity of the karst subsurface, including variations in fracture aperture, depth, and degree of soil infill, contributes to the limited mixing among these water pools and reinforces their functional separation.~~

Our study reveals significant isotopic variability in fracture water across different depths and fracture apertures (Figs. ~~A4a~~ B4a and ~~A4b~~B4b). In the 0-200cm depth range, the Lc-excess values of fracture water are close to 0‰, with many values even falling below 0‰, reflecting the influence of recent rainfall inputs coupled with kinetic fractionation due to near-surface evaporation.~~indicating that this range of fracture water receives more recent rainfall replenishment and experiences weaker evaporation effects~~. Conversely, ~~However,~~ deep fracture water at depths greater than 200 cm typically has Lc-excess values above 0‰~~,~~. These signatures suggest that deeper fracture water is largely decoupled from surface evaporative processes and is likely derived from infiltration events that preserve the original isotopic composition of precipitation.~~suggesting that deep fracture water has undergone a longer storage and vapor exchange process, with water sources being long-term precipitation retention or underground replenishment.~~ More importantly, our data reveal a clear structure-dependent threshold behavior governing water availability.~~Additionally, the aperture of the fractures also significantly affects the isotopic characteristics of the water.~~ Fracture aperture further influences the isotopic characteristics of stored water. Fracture water within narrow apertures (0.5–2 mm) displays a wide range of δD and $\delta^{18}O$ values that exceed the isotopic variability observed in plant xylem water. This variability indicates that water stored in small fractures is more susceptible to mixing processes and variable evaporative fractionation.~~Fracture water with apertures between 0.5 and 2 mm exhibits a wide range of δD and $\delta^{18}O$, exceeding the isotopic variation range of xylem water in vegetation. This indicates that the water in these fractures has undergone more complex replenishment and migration processes influenced by soil water, precipitation infiltration, and evaporation~~

带格式的: 缩进: 首行缩进: 2 字符

设置了格式: 字体: (中文) +中文正文 (DengXian)

设置了格式: 上标

fractionation. In contrast, fracture water within larger apertures (10–38 mm) falls largely within the isotopic range of xylem water and shows Lc-excess values closer to those of plant water. These patterns indicate that larger fractures, particularly those containing soil infill, can reduce evaporative enrichment and slow water exchange with the surrounding matrix. Previous work has shown that soil infill can substantially modify fracture hydraulic properties Meanwhile, fracture water with apertures between 10 and 38 mm has isotopic values within the range of xylem water, and its Lc-excess is less than 0‰ — closer to xylem water, suggesting that such fracture water serves as a stable water source for vegetation. (Liu et al., 2024b), increasing water retention and creating relatively stable subsurface water stores that may support plant water uptake.

Fracture water at 600 cm depth shows more concentrated δD and $\delta^{18}O$ values, with a much narrower isotopic range than xylem water. Therefore, if this deep fracture water is used to represent root zone fracture water for vegetation water source partitioning, it may fail to explain the entire water utilization strategy of vegetation and lead to errors. Many studies that use deep spring water (Ding et al., 2021; Rong et al., 2011; Fan et al., 2023; Deng et al., 2015; Nie et al., 2012; Cai et al., 2023; Wu et al., 2021; Carrière et al., 2020; Wu et al., 2024b; Zeng et al., 2021; Cai et al., 2025), or mixed borehole water (Deng et al., 2020) as epikarst zone water for vegetation water source partitioning may introduce uncertainty in identifying the actual water sources used by plants are not rigorous.

Our findings suggest that analyses of plant water use in karst systems should explicitly consider fracture structural properties (e.g., aperture, depth, and infill porosity) when defining rock water sources, in order to better resolve water partitioning within the coupled soil-plant-rock fracture continuum. Our findings suggest that research on vegetation water use in karst regions should consider the impact of different fracture depths and apertures, as the heterogeneity of fracture spaces can lead to significant variations in isotopic composition.

Our findings suggest that accurate analysis of plant water use and ecohydrological separation in karst systems must explicitly incorporate rock water into the water source framework. This is to account for seasonal water source shifts under varying hydroclimatic conditions and to fully understand the functioning of the coupled soil-plant-rock fracture continuum.

4.2 On the surprising similarity between mobile soil water and bulk soil water

Our isotopic correlations between bulk soil water and mobile soil water. (Fig. A5 B5) shows that during dry seasons (February-May and October-January), the correlation between the isotopic values of bulk soil water and mobile water is weak (R^2 = 0.002-0.34). This indicates poor hydraulic coupling between the two components. Notably, the isotopic values of bulk water (obtained using the CVD method) are more depleted than those of mobile water (using suction lysimeters). This is consistent with the initial findings of Brooks et al. (2010) and follow-up work by Sprenger et al. (2019), Zhao and Wang (2021) and Xu et al. (2025). Brooks et al. (2010) conducted their study in a Mediterranean climate within the western Cascade Mountains of Oregon, USA. In the H. J. Andrews Experimental Forest, they collected samples during the dry season (June, August, September 2004-2005) and the wet-up period in autumn 2006 (October-December). Across these campaigns, Brooks et al. (2010) found that the weak isotopic correlation between bulk and mobile water suggests limited mixing, likely resulting from their residence in different pore domains. This implies that during these periods, bulk and mobile water are influenced

by distinct recharge sources and subject to different degrees of evaporation-driven isotopic fractionation, thereby enhancing ecohydrological separation.

However, in our study, we observed that during the high-rainfall period in June- September, this separation effect becomes less pronounced. The correlation between bulk and mobile soil water isotopic values improves markedly (R^2 = 0.60-0.61; Fig. ~~A5~~B5), indicating that recent precipitation inputs increasingly dominate the mobile water pool and that some degree of hydraulic exchange occurs between the two compartments. This seasonal shift suggests a dynamic and partial coupling between soil water pools under high moisture conditions, which may temporarily weaken ecohydrological separation (Geris et al., 2015). Snelgrove et al. (2021) report that in a catchment in northern Britain, high soil water storage and limited precipitation inputs in humid settings can facilitate mixing between soil water and mobile water, reducing the likelihood of pronounced separation. Similarly, in ecosystems with high rainfall and elevated soil moisture, such as tropical rainforests, the isotopic differences between soil water and plant xylem water are often small or even negligible, indicating little to no separation (Liu et al., 2020). Ecohydrological separation is more likely during dry periods and tends to weaken or disappear during the wet season (Luo et al., 2019; Hervé-Fernández et al., 2016).

To further investigate the hydraulic linkage of different water components at varying depths, we analyze isotopic relationships stratified by depth. The results show that in the upper 0-50 cm layer, the correlation between soil bulk and mobile water is relatively strong (R^2 = 0.68-0.78), whereas in the 50-200 cm layer, the correlation weakens significantly (R^2 = 0.32-0.46; Fig. 7). Vargas et al. (2017) demonstrated that under wet conditions, 75-95% of mobile water can exchange isotopically with surrounding bound water in the upper soil layers (< 30 cm).

Fig. ~~A6~~ B6 further reveals that with increasing depth, mobile soil water becomes increasingly enriched in δD and $\delta^{18}O$, while its isotopic range remains relatively stable, and Lc-excess values remain near 0‰. In contrast, bulk soil water shows a gradual depletion in δD and $\delta^{18}O$ with depth, along with significantly lower Lc-excess values, aligning more closely with xylem water.

These findings suggest that in surface soils, precipitation infiltrates rapidly and alters the isotopic composition of both mobile and bulk soil water, while also enhancing hydraulic connectivity between different pore domains. This is particularly evident during periods of intense rainfall, when high soil moisture content reduces matric potential gradients and facilitates lateral and vertical water exchange across pore domains. Under such conditions, even tightly bound water may undergo partial displacement or mixing due to sustained infiltration and elevated hydraulic gradients.

With increasing depth, however, the hydraulic connection between bulk and mobile water progressively weakens. Deep bulk water increasingly behaves as a relatively isolated reservoir, with limited exchange, while mobile water remains hydrologically dynamic and responsive to recent precipitation inputs through preferential flow pathways. This vertical stratification in hydraulic behavior results in the clear manifestation of ecohydrological separation within the soil profile under most seasonal conditions.

Nevertheless, during the peak rainy season, the high volume and intensity of precipitation enhance water fluxes and recharge rates throughout the profile. This leads to greater pore connectivity and transient mixing between bulk and mobile

water pools, thereby weakening the separation effect. Thus, our findings demonstrate that ecohydrological separation is not static but modulated by seasonal hydrological regimes, with stronger separation under drier conditions and partial coupling during wetter periods when hydrodynamic forces override structural constraints.

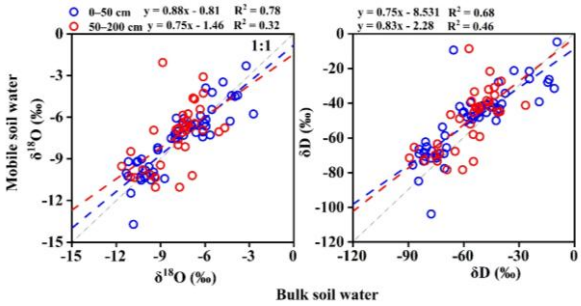

Figure 7. Isotopic comparisons (δD and $\delta^{18}O$) between bulk soil water and mobile water across soil depths.

4.3 A perceptual model for the role of rock fractures in plant water uptake in karst

Our findings lead to a perceptual model that illustrates how plants dynamically access different water sources in karst ecosystems, shaped by the structural and hydrodynamic properties of the soil-rock continuum. The conceptual framework presented in ~~Figure~~ Fig. 8 depicts a vertically stratified water source system composed of four primary compartments: mobile soil water, bulk soil water, rock fracture water, and infilled rock fracture water.

Overall, the preferential water source hierarchy in this karst system follows the order: mobile soil water > bulk soil water > rock water. In our study, mobile water is characterized by short residence times and high turnover. Mobile soil water is the primary support for transpiration during wet periods but is less accessible during dry spells. In contrast, bulk soil water, with its longer MRT, is mainly used by vegetation during the late growing season and senescence period. Rock water, especially that stored in soil-filled fractures, with its longer MRT and higher retention capacities, acts as a more stable source, sustaining plant function when soil water is depleted, thereby substantially enhancing tree survival and transpiration stability during drought periods and facilitating the onset of the growing season (Hahm et al., 2022; Leite et al., 2025; Schwinning, 2020).

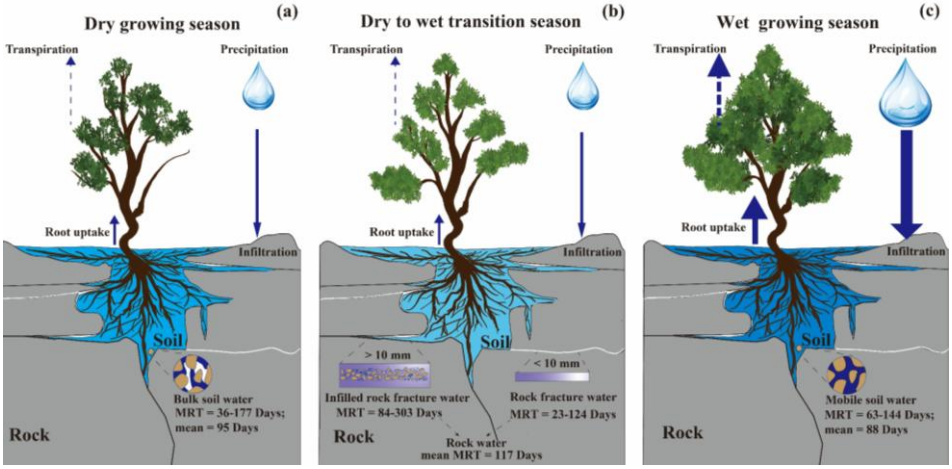

Figure 8. Perceptual model of the plant water uptake from the root zone in karst.

Specifically, precipitation infiltrates the thin soil layer and preferentially recharges mobile soil water stored in connected pores. This water is readily available for root uptake but has a short residence time and low retention capacity, particularly during the wet season (peak growing season). As water percolates downward, part of it is retained in micropores as bulk soil water, which is replenished more slowly and supports vegetation during ~~moderately dry periods~~late growing season and senescence period. At greater depths, plant roots interact with the weathered bedrock. Rock fractures with smaller apertures and minimal soil infill function as transient water storage compartments with intermediate MRT, whereas larger fractures that are substantially filled with soil serve as long-term reservoirs, characterized by significantly prolonged water retention (MRT up to 303 days in our study). These fractures are crucial for maintaining transpiration during dry or transitional periods (e.g., reactivation period~~early spring~~ and early growing season~~late fall~~), especially for large, deep-rooted trees. Our isotope and MRT analyses show that vegetation flexibly shifts water use based on seasonal availability, progressively relying on infilled rock fracture water and bulk soil water as mobile soil water becomes scarce.

In Southwest China, long-term anthropogenic disturbances and natural processes have driven extensive karst desertification, resulting in severe soil degradation, vegetation loss, and ecosystem instability (Wang et al., 2019b). Despite a general "greening" trend since 2000 (Tong et al., 2018), projections indicate that drought frequency in Southwest China is likely to increase further between 2021 and 2035 (Climate Change Assessment Report for Southwest China, 2021). A combination of reduced precipitation, rising temperatures, more frequent and intense droughts, soil degradation, and insufficient water resource management may amplify the vulnerability of current forest restoration efforts (Peng et al., 2020; Zhou et al., 2020; Lin et al., 2015; Zhao et al., 2024), affecting plant water uptake and long-term ecosystem stability. With

global warming intensifying the hydrological cycle, shifts between wet and dry periods are becoming more pronounced (He et al., 2024; Chen et al., 2025). It is projected that by 2040-2100, nearly 60% of the global land surface will experience accelerated dry-wet transitions (Chen and Wang, 2022). The frequency of both atmospheric drought and surface soil drought is rising (Xu et al., 2024; Fabiani et al., 2024), which may lead to fundamental changes in plant water-use strategies (Wei et al., 2023; Salomón et al., 2022). Under such conditions, rock fracture water may serve as a crucial buffer, sustaining vegetation during drought events (Schwinning, 2020; Korboulewsky et al., 2020; Luo et al., 2024b; Wu et al., 2024a). However, current research has not adequately elucidated the regulatory mechanisms by which soil-rock structures control water transport and retention times, nor their influence on vegetation water uptake. In particular, there is a lack of quantitative, mechanistic studies focusing on factors such as fracture aperture, soil-filled fractures, soil physical properties, and the interactions between vegetation and the soil-rock structure.

More broadly, our framework highlights the underappreciated role of rock fracture water in sustaining vegetation function under increasing climate variability. Future ecohydrological modeling and karst forest restoration should explicitly incorporate the structure and hydrodynamics of the soil-rock continuum to improve resilience and adaptive capacity in these fragile landscapes.

5. Conclusion

Our study represents one of the first mechanistic investigations into the role of rock fractures in facilitating rock moisture uptake by plants in karst environments. By integrating stable isotope analysis with MRT modeling, we delineated four functionally distinct water compartments within a structurally heterogeneous soil-rock continuum: mobile soil water, bulk soil water, rock fracture water, and infilled rock fracture water. Our results demonstrate that plant water uptake strategies are seasonally modulated by the availability and hydrodynamic behavior of these compartments. Notably, vegetation exhibits a clear preference for water sources with shorter MRTs, especially under wetter conditions. During the ~~wet~~ peak growing season, rainfall-driven mobile soil water predominates in supporting plant transpiration. In contrast, during ~~dry~~ no growing or transitional ~~period~~seasons, trees increasingly ~~relies~~ rely on bulk soil water and rock fracture water, particularly from infilled fractures characterized by longer MRTs (84-303 days). The limited mixing and distinct MRTs observed among these water pools are largely consistent with the premise of the ecohydrological separation hypothesis. ~~The limited mixing and distinct MRTs observed among these water pools provide strong support for the ecohydrological separation hypothesis.~~ However, under high moisture conditions, increased hydraulic connectivity appears to reduce this separation. The perceptual model developed from this work highlights the critical buffering role of rock fracture water in sustaining vegetation under variable hydroclimatic regimes. These findings underscore the importance of incorporating bedrock heterogeneity, water source dynamics, and seasonal shifts in plant water use into ecohydrological models of karst systems. Given the anticipated increases in drought frequency and climatic variability, future forest management and restoration strategies in karst landscapes should explicitly consider the integrated behavior of the soil-rock-plant continuum to enhance ecosystem resilience.

Appendix A

Table A1. Summary of soil moisture monitoring and soil water sampling design across study sites.

Category		Soil moisture monitoring	Bulk soil sampled	Mobile soil water sampled
Dates		Sep 2022 – Jun 2025	Apr 2024–Mar 2025	Sep 2022–Nov 2024
Frequency		30 min	Dry season: once per month; rainy season: 1–2 times per month	Dry season: once per month; rainy season: 1–4 times per month
Depths at defferent sites (cm)	A	5, 20, 50, 100, 150	5, 20, 50, 70, 100, 150	50, 100
	B	5, 20, 50, 100, 180	5, 20, 50, 70, 100, 180	20, 50, 100, 180
	C & D	5, 20, 40, 50	5, 20, 30, 40, 50	20, 40, 50
	E	5, 30, 50, 100	5, 30, 50, 70, 100	30, 100

875

Table A2. Summary of ~~R~~rock moisture monitoring and rock water sampling design across study sites.

Category		Rock moisture monitoring	Rock water sampled
Dates		Sep 2022–Jun 2025	Sep 2022–Mar 2025
Frequency		30 min	Dry season: once per month; rainy season: 1–4 times per month
Depths at defferent sites (cm)	A	20, 62, 105, 147, 220, 270	62, 147, 270, 600
	B	45, 50, 60, 80, 100, 150, 180	45, 50, 60, 80, 100, 150, 180
	C & D	20, 40, 79, 94, 165, 176, 200, 244, 306	79, 94, 165, 176, 200, 244, 306
	E	170, 207	170, 207, 248
Fracture apertures at defferent sites (mm)	A	0.54, 0.8, 0.92, 1.89, 3.06, 6.45	1.89, 3.06, 5, 6.45
	B	0.47, 0.5, 0.55, 1.43, 10, 15, 21	0.47, 0.5, 0.55, 1.43, 10, 15, 21
	C & D	0.16, 0.2, 0.26, 2, 20, 30, 35, 38	0.16, 0.26, 2, 20, 30, 35, 38
	E	2.4, 2.6	1.84, 2.4, 2.6

Table A3. Summary of tree-based sampling design and root-zone characteristics across study sites.

Site	Tree number	Species	Characteristics of root zone			Characteristics of trees			
			Soil depth (cm)	Soil volume (m^3)	Fracture volume (m^3)	Height (m)	DBH (cm)	Canopy area (m^2)	Sapwood area (cm^2)
A	bp_1	*Broussonetia papyrifera* (L.) L'Hér. ex Vent.	200	1.68	1.30	7.00	29.60	62.83	499
	bp_2		200	0.67	0.52	7.00	12.80	25.04	82.60

设置了格式: 字体: 9 磅, 加粗
设置了格式: 字体: 9 磅, 加粗
设置了格式: 字体: 10 磅, 非加粗
设置了格式: 字体: 10 磅, 非加粗
设置了格式: 字体: 10 磅, 非加粗
带格式的: 居中, 行距: 多倍行距 1.15 字行
格式化表格
带格式的: 居中, 行距: 多倍行距 1.15 字行
带格式的: 行距: 多倍行距 1.15 字行
带格式的: 行距: 多倍行距 1.15 字行
带格式的: 居中, 行距: 多倍行距 1.15 字行
格式化表格
带格式的: 居中, 行距: 多倍行距 1.15 字行
带格式的: 居中, 行距: 多倍行距 1.15 字行
设置了格式: 字体: 10 磅
设置了格式: 字体: 10 磅
设置了格式: 字体: 10 磅
带格式的: 居中, 行距: 多倍行距 1.15 字行
设置了格式: 字体: 10 磅
设置了格式: 字体: 10 磅
设置了格式: 字体: 10 磅
设置了格式: 字体: 10 磅
设置了格式: 字体: 10 磅
设置了格式: 字体: 10 磅
设置了格式: 字体: 10 磅
格式化表格

Site	Tree number	Species	Characteristics of root zone			Characteristics of trees			
			Soil depth (cm)	Soil volume (m^3)	Fracture volume (m^3)	Height (m)	DBH (cm)	Canopy area (m^2)	Sapwood area (cm^2)
	bp_3		200	1.26	0.98	7.00	22.00	47.12	219
B	ts_1	*Toona sinensis* (A.Juss.) M.Roem.	43	1.12	0.04	5.50	5.40	1.30	18.36
	ts_2		22	0.42	0.05	5.80	5.80	1.51	19.23
C	ts_5	*Toona sinensis* (A.Juss.) M.Roem.	16	0.12	0.61	11.50	10.77	14.00	34.19
	ts_6		60	6.88	2.19	12.35	36.00	50.46	593
	cc_3	*Cinnamomum camphora* (L.) J.Presl.	52	0.71	0.95	7.00	11.73	21.90	59.24
	yd_1	*Yulania denudate* (Desr.) D.L.Fu	53	0.37	0.44	6.00	9.63	10.07	38.45
	yd_2		52	1.42	0.33	7.00	12.75	7.52	16.34
D	ts_3	*Toona sinensis* (A.Juss.) M.Roem.	24	0.22	1.01	10.50	10.00	10.40	31.27
	ts_4		60	0.32	1.33	10.50	9.50	13.70	29.52
	cc_1	*Cinnamomum camphora* (L.) J.Presl.	24	0.22	1.65	10.00	13.40	17.01	96.54
	cc_2		30	0.68	1.50	8.00	14.39	15.47	128
E	bp_4	*Broussonetia papyrifera* (L.) L'Hér. ex Vent.	100	2.40	0.38	6.70	16.00	28.04	116.50
	bp_5		15	0.15	0.41	6.50	13.30	30.68	87.26
	kp_1	*Koelreuteria paniculate* Laxm.	20	0.19	0.06	7.00	8.00	4.24	30.44
	kp_2		20	0.18	0.04	5.80	6.80	2.83	23.12

Figure A1. Field photographs illustrating soil and rock water sampling procedures. (a) Vertical boreholes drilled at sites C, D, and E with water sampling devices installed at predefined depths. (b) Horizontal boreholes drilled into exposed bedrock outcrops at sites A and B with sampling devices installed within the soil-rock profile. (c) Collection of soil samples for laboratory extraction of bulk soil water. (d) Collection of mobile soil water using suction lysimeters installed in soil layers. (e) Collection of rock fracture water from narrow fractures (aperture approximately 0.1–10 mm) with little or no soil infill. (f) Collection of infilled rock fracture water from wider fractures (>10 mm aperture) largely filled with soil or fine sediments.

设置了格式: 字体: 9 磅, 加粗, 字体颜色: 文字 1

设置了格式: 字体: 10 磅, 加粗, 字体颜色: 文字 1

Appendix ~~A~~B

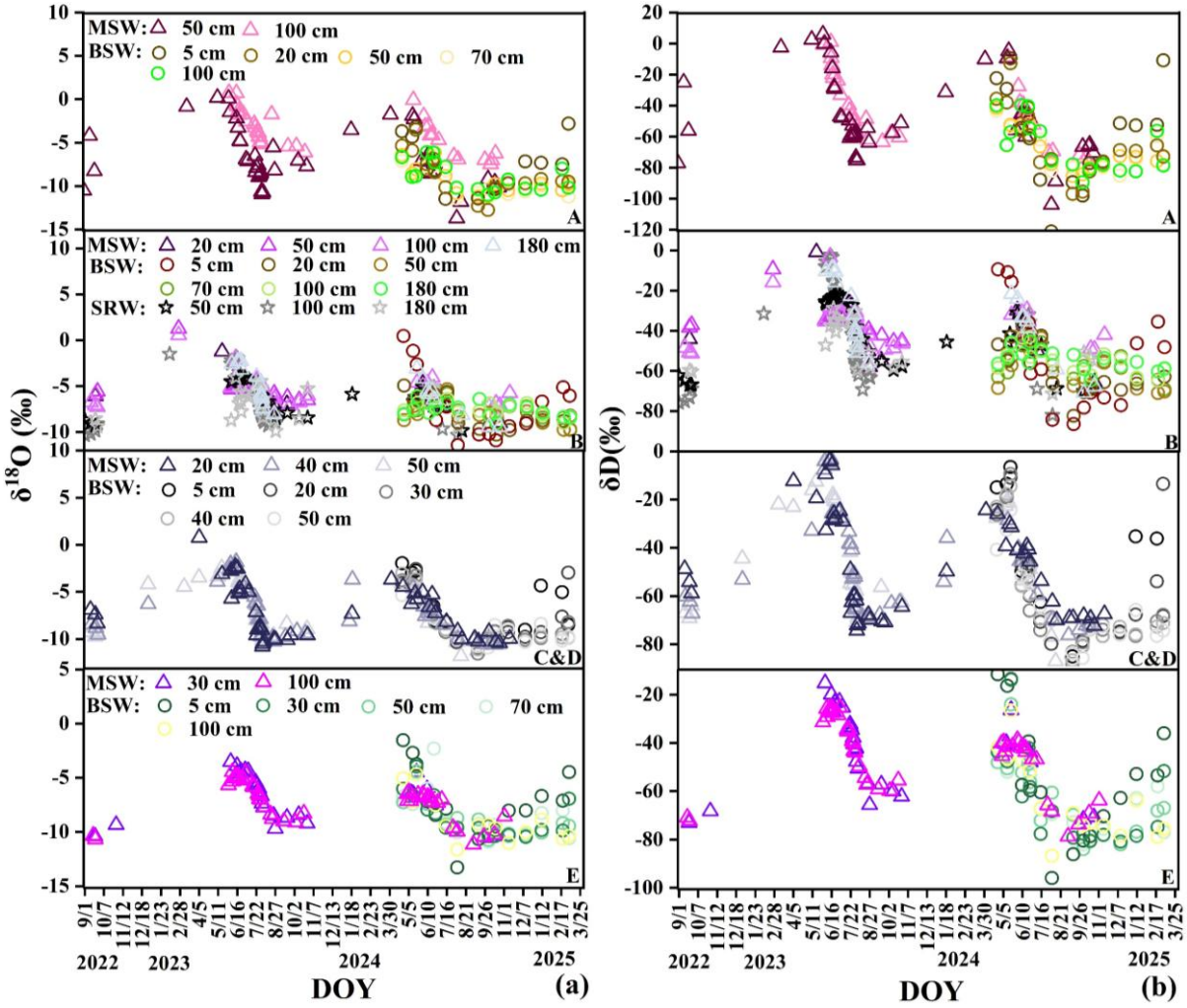
MSW: 50 cm 100 cm
BSW: 5 cm 20 cm 50 cm 70 cm
100 cm
A
MSW: 20 cm 50 cm 100 cm 180 cm
BSW: 5 cm 20 cm 50 cm
70 cm 100 cm 180 cm
SRW: 50 cm 100 cm 180 cm
B
MSW: 20 cm 40 cm 50 cm
BSW: 5 cm 20 cm 30 cm
40 cm 50 cm
C&D
MSW: 30 cm 100 cm
BSW: 5 cm 30 cm 50 cm 70 cm
100 cm
E
δ18O (‰)
δD(‰)
2022 2023 2024 2025
DOY
(a)
(b)

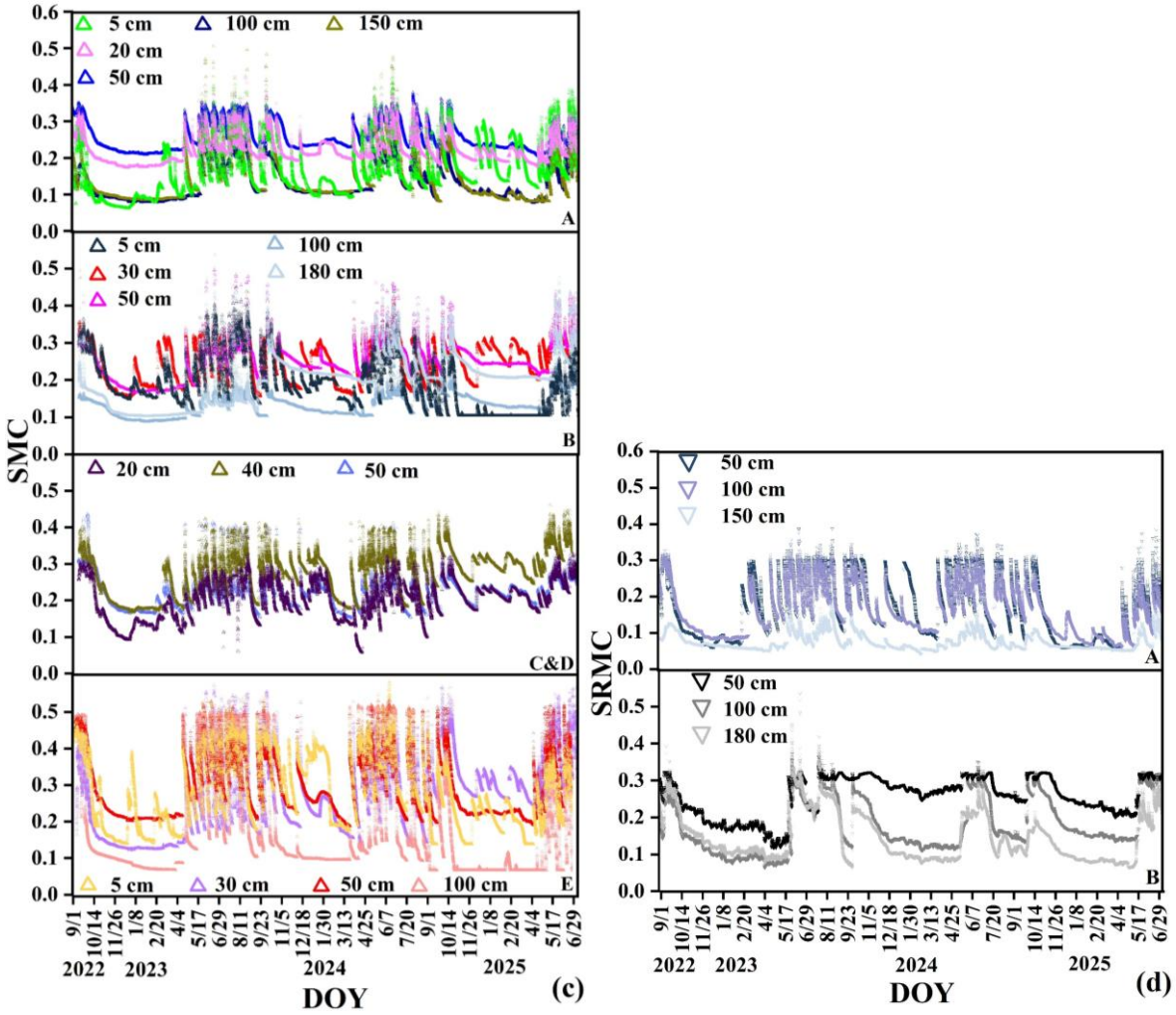

890 **Figure ~~A~~B1. Dynamic variations in stable isotopes of soil water at different depths at sites (A-E): (a) $\delta^{18}O$ and (b) δD, and moisture content: (c) and (d). Mobile soil water (MSW), bulk soil water (BSW), soil-rock interface water (SRW), soil moisture content (SMC), soil-rock interface moisture content (SRMC).**

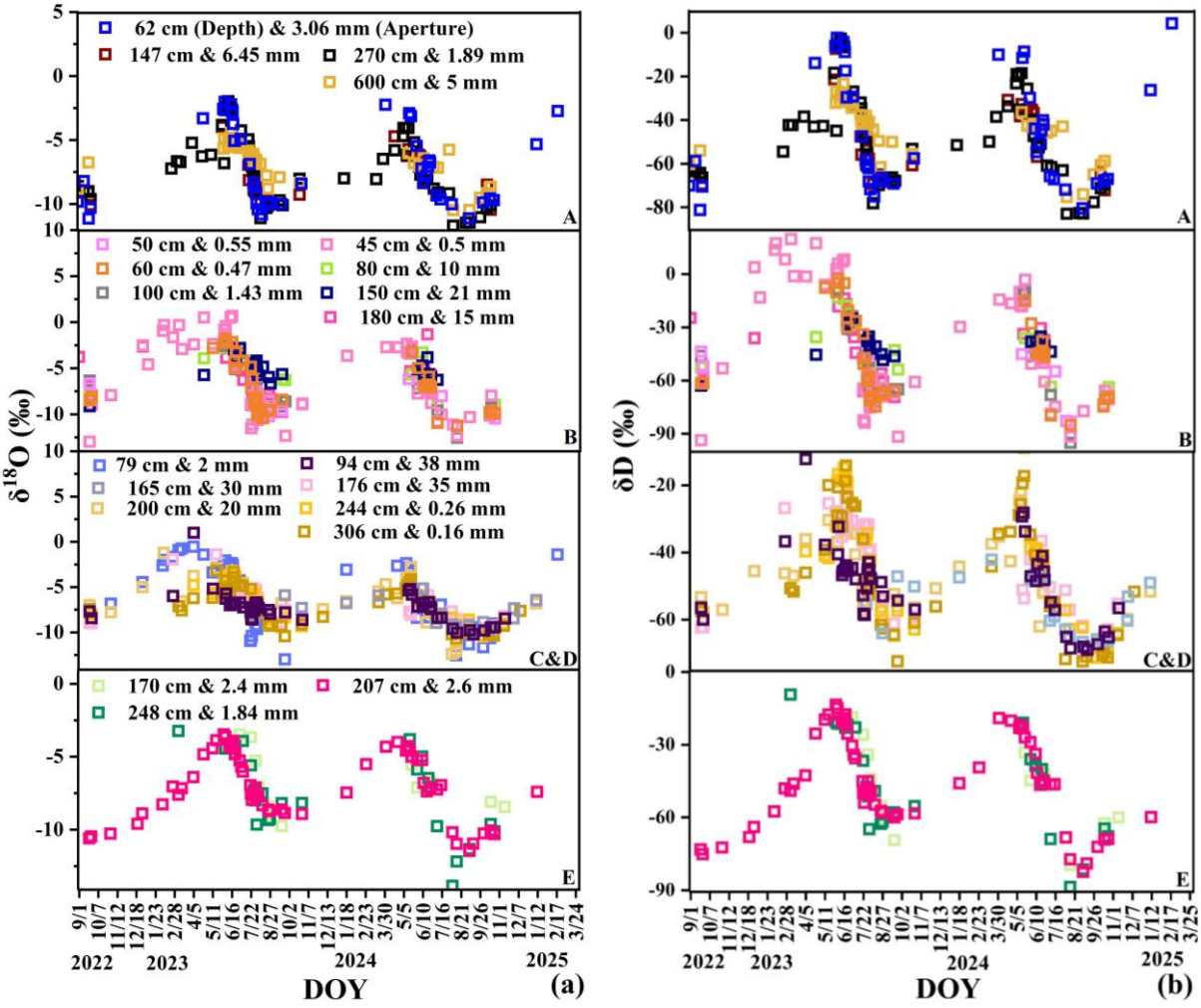
62 cm (Depth) & 3.06 mm (Aperture)
147 cm & 6.45 mm
270 cm & 1.89 mm
600 cm & 5 mm
A
50 cm & 0.55 mm
60 cm & 0.47 mm
100 cm & 1.43 mm
45 cm & 0.5 mm
80 cm & 10 mm
150 cm & 21 mm
180 cm & 15 mm
B
79 cm & 2 mm
165 cm & 30 mm
200 cm & 20 mm
94 cm & 38 mm
176 cm & 35 mm
244 cm & 0.26 mm
306 cm & 0.16 mm
C&D
170 cm & 2.4 mm
248 cm & 1.84 mm
207 cm & 2.6 mm
E
δ18O (‰)
δD (‰)
DOY
2022
2023
2024
2025
(a)
(b)

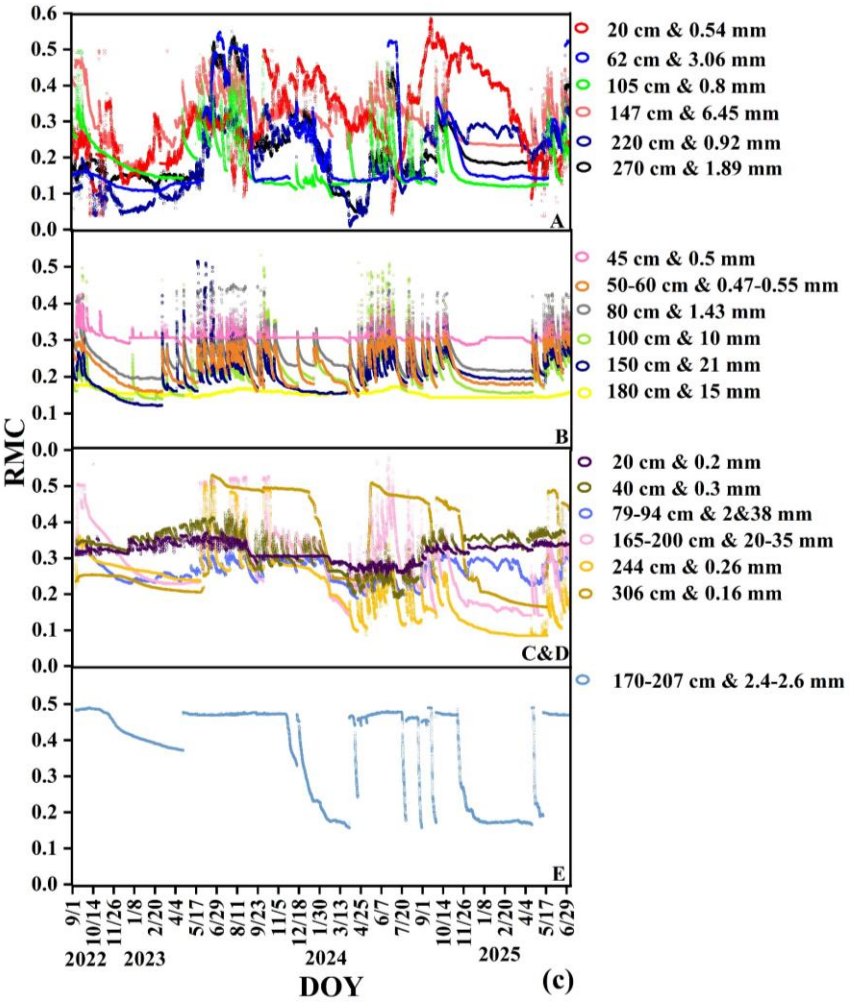

Figure ~~A2~~B2. Dynamic variations in stable isotopes of rock fracture water at different depths / apertures at sites (A-E): (a) $\delta^{18}O$ and (b) δD, and moisture content: (c).

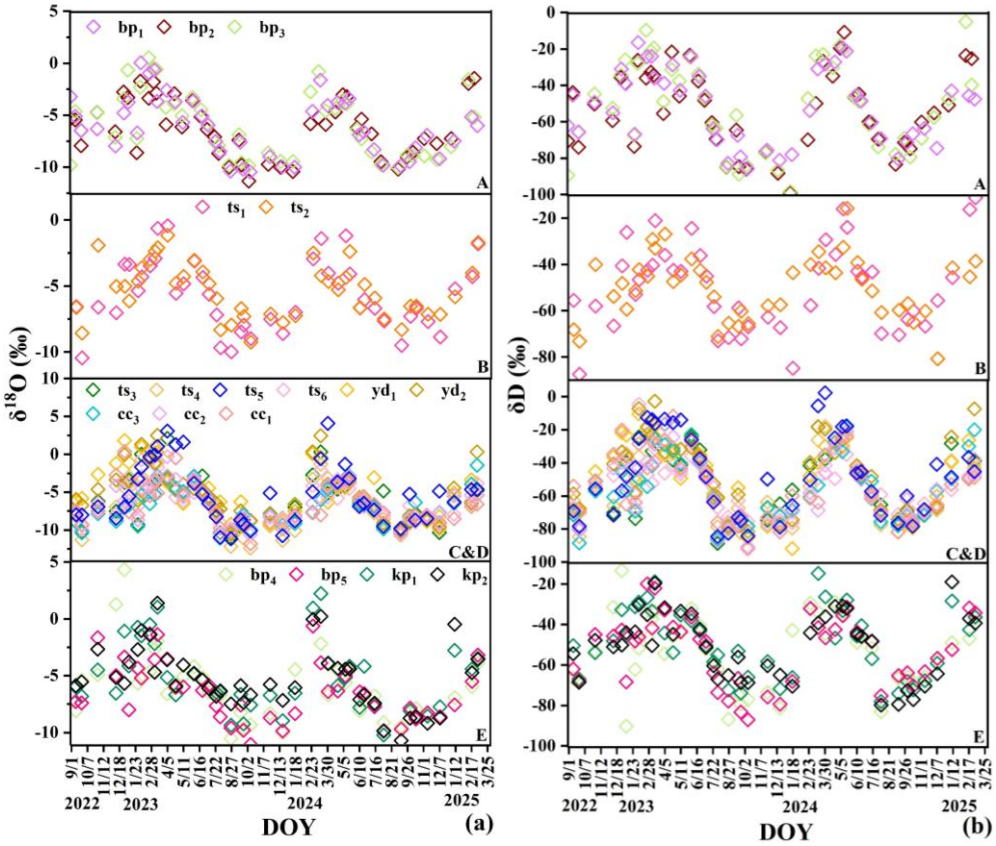

Figure ~~A3~~B3. Dynamic variations in stable isotopes of xylem water (δD and $\delta^{18}O$) in different trees at sites (A-E).

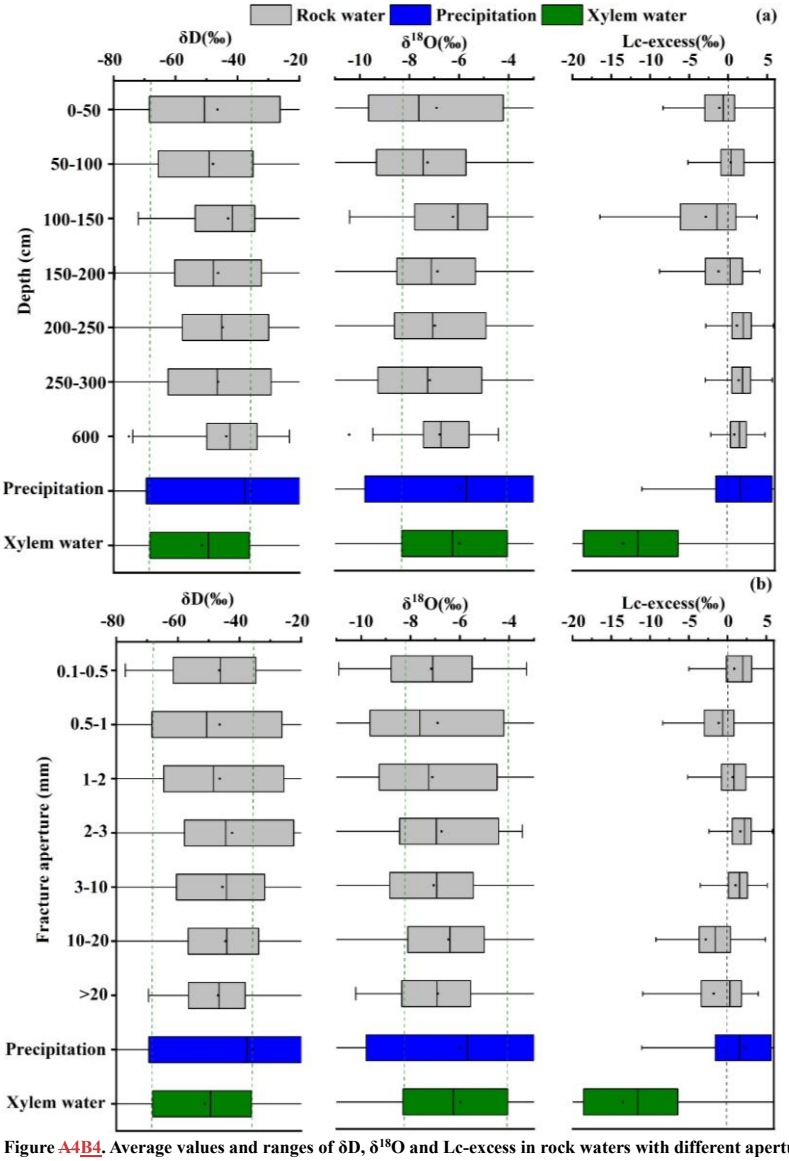

900

Figure A4B4. Average values and ranges of δD, $\delta^{18}O$ and Lc-excess in rock waters with different apertures.

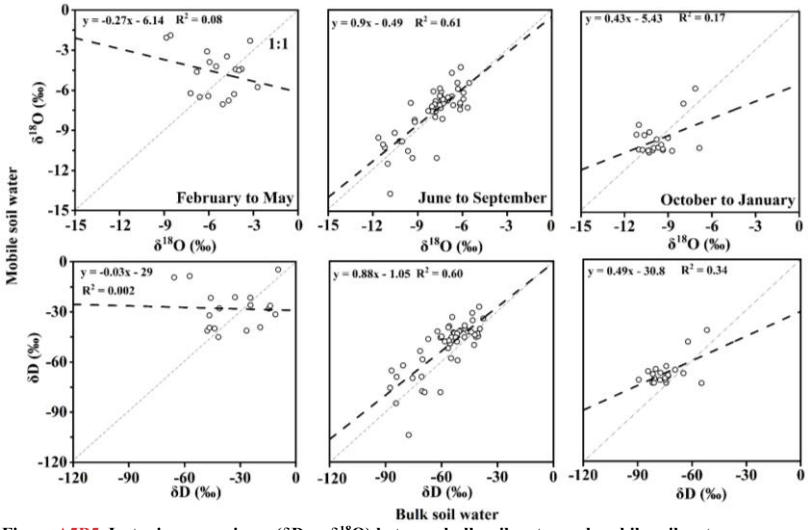

Figure ~~A5~~B5. Isotopic comparisons (δD or $\delta^{18}O$) between bulk soil water and mobile soil water.

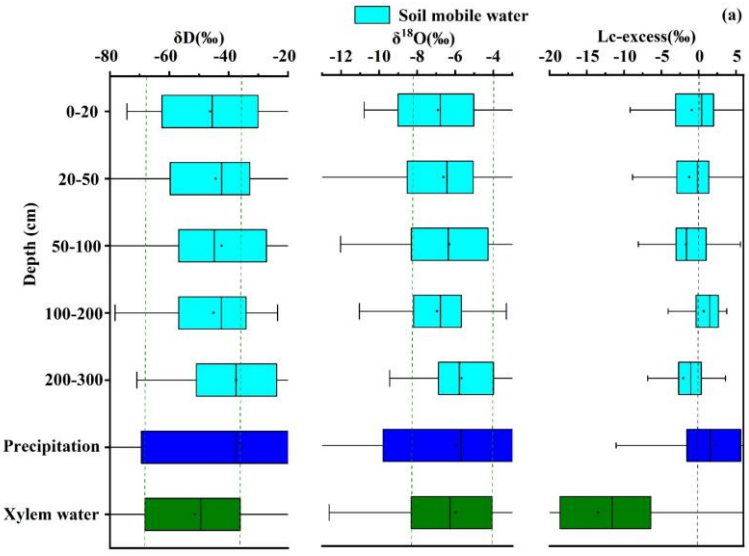

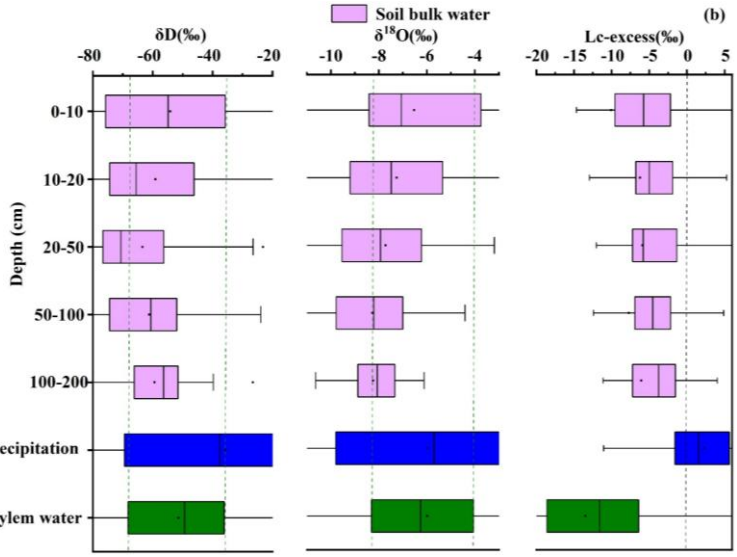

Figure ~~A6~~B6. Average values and ranges of δD, $\delta^{18}O$ and Lc-excess in different soil waters.

Appendix ~~B~~C

To distinguish it from mean residence time (MRT), we applied the mean transit time (MTT) phase shift method from Allen et al. (2018) to quantify the time delay in water transport between compartments. The phase shift primarily captures the time lag between input signals (e.g., precipitation isotopic composition) and output signals (e.g., plant or groundwater isotopic composition). MTT represents the time lag or transmission time between different compartments in the hydrological cycle (e.g., precipitation to soil, soil to rock, rock to plant). ~~(Liu et al., 2024c)~~

The MTT (in day) calculation was made by:

$$MTT = c^{-1}(\phi_w - \phi_p) \quad (C\text{~~B~~}1)$$

Where $c = 2\pi \cdot 365^{-1}$ is the angular frequency constant, which represents the yearly cycle (assuming a one-year period for seasonal variations); ϕ_p is the phases of precipitation sine curves, and ϕ_w is water sine curve (mobile soil water, bulk soil water, rock fracture water, infilled rock fracture water, soil-rock interface water and xylem water).

Table ~~B1~~ C1 shows MTT was positively correlated with MRT (MTT = 19.55ln(MRT) - 66, $R^2 = 0.77$), with a range of 6-82 days and an average of 28 days. Site B also exhibited significantly higher MTT values (10-82 days, mean 39 days) compared to other sites (6-38 days, mean 21 days). Data in Tables C1–3 consistently show that MRT exceeds MTT. This disparity reflects that the two metrics describe different aspects of water age dynamics within the same compartment. MTT is derived from the phase shift of the seasonal isotope signal and therefore represents the timing of signal propagation between connected compartments. In contrast, MRT is derived from amplitude damping and reflects the persistence of water within a reservoir as controlled by storage volume and internal mixing. Because subsurface storage and mixing can substantially attenuate isotope amplitudes without proportionally delaying signal transmission (due to preferential flow pathways), MRT is typically longer than MTT. Despite this difference in magnitude, the positive relationship between MRT and MTT indicates that subsurface structural properties coherently influence both transport delay and storage persistence.

Table C4 details both the MRT and MTT for different water sources utilized by trees. Here, MRT (derived from amplitude damping) characterizes the mixing volume and turnover time of water within the tree-source system (storage), while MTT (derived from phase shift) quantifies the time lag for water to be transported from the soil/rock source to the tree xylem (uptake delay). Negative MTT values occur when the isotope signal in plant xylem precedes that of water sources. This does not indicate negative physical transport time, but rather reflects the dominance of older or deeper water pools in plant uptake, where isotope signals are seasonally advanced due to prior recharge or long-term storage (Liu et al., 2024c).

Table ~~B1~~C1. Statistics of MRT and MTT (day) for mobile and bulk water in different soil layers.

Site	Depth (cm)	K_h (cm·h^{-1})	Average moisture content	Mobile soil water					Bulk soil water				
				MRT	MTT	Number of samples	R^2	Standard error	MRT	MTT	Number of samples	R^2	Standard error
A	5	3.83	0.153	-	-	-	-	-	36	6	16	0.75	19.08
	20	3.33	0.223	-	-	-	-	-	65	16	16	0.89	11.20
	50	2.33	0.264	72	15	68	0.56	18.15	139	26	16	0.67	8.48
	70	2.18	-	-	-	-	-	-	155	28	16	0.54	8.46
	100	1.96	0.133	74	31	36	0.83	11.77	138	32	16	0.64	9.96
B	5	0.58	0.212	-	-	-	-	-	49	10	16	0.80	11.74
	20	0.44	0.245	63	23	23	0.61	9.35	177	31	16	0.55	9.01
	50	0.16	0.241	459	34	38	0.52	2.09	471	73	16	0.50	9.00
	70	0.17	-	-	-	-	-	-	638	82	16	0.54	6.82
	100	0.18	0.125	244	43	40	0.54	5.34	685	47	16	0.50	5.41
	180	0.10	0.182	77	24	25	0.64	10.59	708	63	16	0.53	4.84
C&D	5	4.96	0.191	-	-	-	-	-	40	6	16	0.78	17.07
	20	1.04	0.261	85	25	51	0.68	12.28	60	12	16	0.81	11.02
	30	1.04	-	-	-	-	-	-	66	9	16	0.83	13.13
	40	1.04	0.209	85	33	45	0.74	11.04	63	12	16	0.87	10.71
	50	1.04	0.209	63	20	49	0.83	11.77	95	17	16	0.93	7.18
E	5	1.42	0.309	-	-	-	-	-	47	8	16	0.83	13.63
	30	0.75	0.227	122	38	33	0.57	9.77	108	19	16	0.68	12.30
	50	0.75	0.298	-	-	-	-	-	131	27	16	0.85	8.95
	70	0.83	-	-	-	-	-	-	118	24	16	0.88	7.79
	100	0.96	0.204	144	32	48	0.50	9.84	121	17	16	0.74	9.41
Mean	51	1.39	0.217	135	29	41	0.64	10.18	196	27	16	0.72	10.25

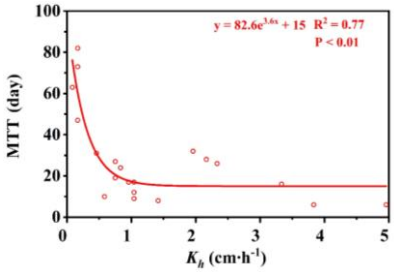

Figure C1. Relationship between K_h and MTT of bulk soil water.

945

Table C2. Statistics of MRT and MTT (day) for soil-rock interface water in different soil layers

Site	Depth (cm)	Average moisture content	MRT	MTT	Number of samples	R^2	Standard error
B	50	0.254	119	39	46	0.57	9.23
	100	0.166	21	25	35	0.85	11.69
	180	0.154	214	41	10	0.50	6.68
Mean	110	0.191	118	35	30	0.64	9.20

格式化表格
设置了格式

Table ~~B3~~C3. Statistics of MRT and MTT (day) for fractures of different apertures and depths.

Site	Aperture (mm)	Depth (cm)	Porosity (ε_p)	K_h (cm·h^{-1})	Average moisture content	MRT	MTT	Number of samples	R^2	Standard error
C&D	0.16	306	1	0.09	0.354	124	31	54	0.56	11.30
C&D	0.26	244	1	1.13	0.256	118	34	43	0.63	10.80
B	0.47	60	1	3.04	0.217	57	24	44	0.72	14.04
B	0.50	45	1	3.42	0.310	23	-2	30	0.70	17.44
B	0.55	50	1	3.71	0.217	91	25	59	0.50	17.77
B	1.43	80	0.98	17	0.260	76	22	34	0.64	14.03
E	1.8	248	0.75	13	-	73	20	34	0.72	14.84
A	1.89	270	0.98	673	0.217	108	30	61	0.61	14.62
C&D	2	79	0.74	76	0.256	35	2	60	0.73	15.13
E	2.4	170	0.6	34	0.413	103	29	23	0.55	12.06
E	2.6	207	0.54	47	0.413	97	33	70	0.75	10.23
A	3.06	62	0.80	40	0.203	60	22	44	0.69	13.90
A	5	600	0.66	3496	-	182	29	47	0.50	6.21
A	6.45	147	0.55	6208	0.317	100	24	38	0.69	9.75
B	10	100	0.41	6	0.206	136	27	38	0.55	12.20
B	15	180	0.45	33	0.158	84	21	44	0.57	12.85
C&D	20	200	0.47	315	0.311	176	25	53	0.60	8.63
B	21	150	0.74	1042	0.188	~~136~~198	~~27~~38	25	0.55	12.20
C&D	30	165	0.49	87	0.311	303	20	25	0.54	6.90
C&D	35	176	0.74	2232	0.311	169	38	43	0.50	9.22
C&D	38	94	0.70	2746	0.256	200	24	50	0.61	6.23
Mean	9.41	173	0.74	813	0.272	120	25	44	0.61	11.92

Table ~~B4~~C4. Statistics of MRT and MTT (day) for different trees at typical sites in the study area.

Site	Tree number	From mobile soil water to tree		From bulk soil water to tree		From rock water to tree		Number of samples	R^2	Standard error
		MRT_1	MTT_1	MRT_2	MTT_2	MRT_3	MTT_3			
A	bp_1	53	-1	58	5	47	-4	45	0.55	13.40
	bp_2	59	5	64	10	53	1	45	0.52	14.70
	bp_3	39	-8	44	-3	31	-12	45	0.57	14.41
B	ts_1	14	0	38	-13	79	3	44	0.52	13.96
	ts_2	40	-7	94	-3	101	-3	44	0.60	10.72
	ts_3	18	-9	60	8	54	7	44	0.63	10.29
	ts_4	22	-10	48	6	51	7	44	0.68	9.07
	ts_5	8	-9	32	7	25	7	44	0.60	10.13
	ts_6	96	2	124	18	128	19	44	0.67	7.78
C&D	cc_1	42	-4	79	13	73	12	44	0.72	11.13
	cc_2	43	-1	80	15	74	14	44	0.72	11.18
	cc_3	45	2	68	19	71	19	44	0.77	11.91
	yd_1	37	-15	60	1	63	2	44	0.54	9.83
	yd_2	29	-12	54	4	57	5	44	0.55	14.51
E	bp_4	13	-21	72	-1	61	-13	44	0.61	12.87
	bp_5	26	-21	83	5	52	-11	44	0.68	10.70
	kp_1	25	-33	83	-6	51	-23	44	0.52	15.78
	kp_2	32	-22	88	5	56	-12	44	0.68	12.09
Mean		36	-9	68	5	63	1	44	0.62	11.91

格式化表格
设置了格式

Appendix D

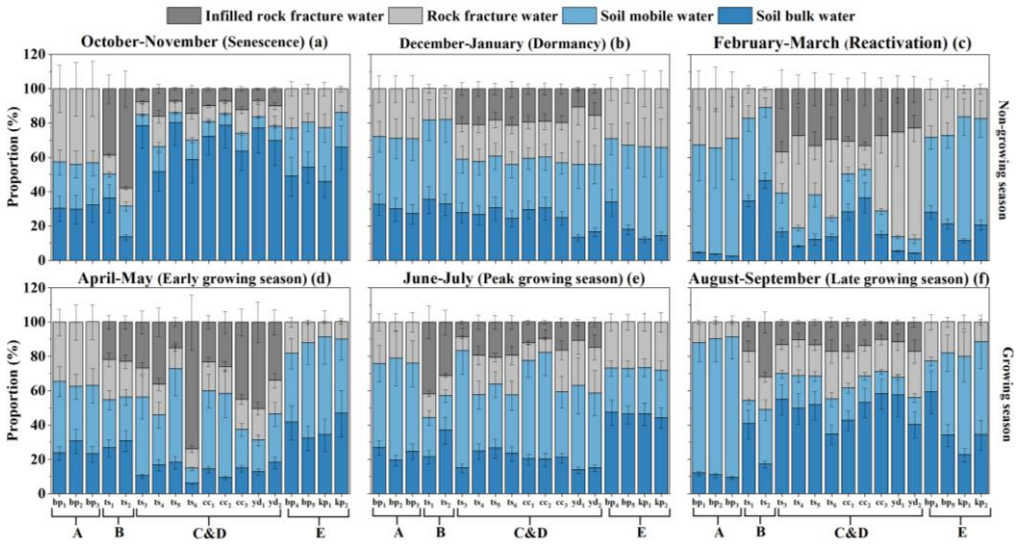

Figure D1. Seasonal variation in the proportional contributions of different water sources to individual tree xylem water across sites. Error bars indicate ±1 standard deviation (SD) derived from the MixSIAR model outputs.

Data availability.

To validate the results of this study and ensure reproducibility, the datasets are accessible on Zenodo (https://zenodo.org/records/14827769, https://zenodo.org/records/16810833) and are publicly available for download (Liu, 2025).

Author contributions.

XL, XC, and JJM conceived the study. XL, WL, and ZZ curated the data. XL and JJM performed the formal analysis. XL and WL carried out the investigation. XL, XC, and JJM developed the methodology. XC, TP, and JJM provided resources. XL developed the software and performed the validation. XL and JJM prepared the original draft. XL, XC, ZZ, and JJM reviewed and edited the manuscript.

Competing interests.

The contact author has declared that none of the authors has any competing interests.

设置了格式: 字体: (默认) Times New Roman, 10 磅, 粗, 字体颜色: 文字 1

带格式的: 标题 2, 行距: 单倍行距

带格式的: 正文

Disclaimer.

Publisher's note: Copernicus Publications remains neutral with regard to jurisdictional claims in published maps and institutional affiliations.

Acknowledgments.

We thank Kim Janzen for conducting all isotopic analyses, and Cody Millar and Hongxiu Wang for their assistance with sample extractions at the University of Saskatchewan. We also gratefully acknowledge Bingcheng Si, Qin Liu and Ha Fu for their valuable comments on the manuscript. The Department of Soil Science at the University of Saskatchewan is thanked for hosting the senior author while the paper was prepared. We thank the Puding Karst Ecosystem Research Station, Chinese Academy of Sciences, for providing field experimental support, and Dr. Jia Chen for kindly sharing the meteorological data. This work was supported by the China Scholarship Council (Grant No. 202306250097).

Financial support.

This research was funded by the National Natural Science Foundation of China (42030506, 42261144672).

References

Allen, S. T., Kirchner, J. W., and Goldsmith, G. R.: Predicting Spatial Patterns in Precipitation Isotope (δ2H and δ18O) Seasonality Using Sinusoidal Isoscapes, Geophysical Research Letters, 45, 4859-4868, https://doi.org/10.1029/2018GL077458, 2018.

Asadollahi, M., Stumpp, C., Rinaldo, A., and Benettin, P.: Transport and Water Age Dynamics in Soils: A Comparative Study of Spatially Integrated and Spatially Explicit Models, Water Resources Research, 56, e2019WR025539, https://doi.org/10.1029/2019WR025539, 2020.

Barbeta, A., Mejía-Chang, M., Ogaya, R., Voltas, J., Dawson, T. E., and Peñuelas, J.: The combined effects of a long-term experimental drought and an extreme drought on the use of plant-water sources in a Mediterranean forest, Global Change Biology, 21, 1213-1225, https://doi.org/10.1111/gcb.12785, 2015.

Bond, B. J., Meinzer, F. C., and Brooks, J. R.: How Trees Influence the Hydrological Cycle in Forest Ecosystems, in: Hydroecology and Ecohydrology, 7-35, https://doi.org/10.1002/9780470010198.ch2, 2008.

Brooks, J. R., Barnard, H. R., Coulombe, R., and McDonnell, J. J.: Ecohydrologic separation of water between trees and streams in a Mediterranean climate, Nature Geoscience, 3, 100-104, https://doi.org/10.1038/ngeo722, 2010.

Cai, L., Xiong, K., Liu, Z., Li, Y., and Fan, B.: Seasonal variations of plant water use in the karst desertification control, Science of The Total Environment, 885, 163778, https://doi.org/10.1016/j.scitotenv.2023.163778, 2023.

Cai, L., Xiong, K., Liu, Z., Li, Y., Zhu, D., Mu, Y., Chen, Y., Zhou, R., and Yan, X.: Water competition among coexisting plants in rock-dominated habitats of subtropical karst desertification, Agriculture, Ecosystems & Environment, 381, 109419, https://doi.org/10.1016/j.agee.2024.109419, 2025.

Carrière, S., Martin-Stpaul, N., Cakpo, C., Patris, N., Gillon, M., Chalikakis, K., Doussan, C., Olioso, A., Babic, M., Jouineau,

A., Simioni, G., and Davi, H.: The role of deep vadose zone water in tree transpiration during drought periods in karst settings – Insights from isotopic tracing and leaf water potential, Science of The Total Environment, 699, 134332, https://doi.org/10.1016/j.scitotenv.2019.134332, 2019.

Carrière, S. D., Martin-StPaul, N. K., Cakpo, C. B., Patris, N., Gillon, M., Chalikakis, K., Doussan, C., Olioso, A., Babic, M., Jouineau, A., Simioni, G., and Davi, H.: The role of deep vadose zone water in tree transpiration during drought periods in karst settings – Insights from isotopic tracing and leaf water potential, Science of The Total Environment, 699, 134332, https://doi.org/10.1016/j.scitotenv.2019.134332, 2020.

Chen, H. and Wang, S.: Accelerated Transition Between Dry and Wet Periods in a Warming Climate, Geophysical Research Letters, 49, e2022GL099766, https://doi.org/10.1029/2022GL099766, 2022.

Chen, H., Liu, J., Wang, K., and Zhang, W.: Spatial distribution of rock fragments on steep hillslopes in karst region of northwest Guangxi, China, CATENA, 84, 21-28, https://doi.org/10.1016/j.catena.2010.08.012, 2011.

Chen, L., Brun, P., Buri, P., Fatichi, S., Gessler, A., McCarthy, M., Pellicciotti, F., Stocker, B., and Karger, D. N.: Global increase in the occurrence and impact of multiyear droughts, Science, 387, 278-284, https://doi.org/10.1126/science.ado4245, 2025.

Darrouzet-Nardi, A., D'Antonio, C. M., and Dawson, T. E.: Depth of water acquisition by invading shrubs and resident herbs in a Sierra Nevada meadow, Plant and Soil, 285, 31-43, https://doi.org/10.1007/s11104-005-4453-z, 2006.

Deng, Y., Kuo, Y.-M., Jiang, Z., Qin, X., and Jin, Z.: Using stable isotopes to quantify water uptake by Cyclobalanopsis glauca in typical clusters of karst peaks in China, Environmental Earth Sciences, 74, 1039-1046, https://doi.org/10.1007/s12665-014-3780-x, 2015.

Deng, Y., Ke, J., Wu, S., Jiang, G., Jiang, Z., and Zhu, A.: Responses of plant water uptake to groundwater depth in limestone outcrops, Journal of Hydrology, 590, 125377, https://doi.org/10.1016/j.jhydrol.2020.125377, 2020.

Deng, Z., Guan, H., Hutson, J., Forster, M. A., Wang, Y., and Simmons, C. T.: A vegetation-focused soil-plant-atmospheric continuum model to study hydrodynamic soil-plant water relations, Water Resources Research, 53, 4965-4983, https://doi.org/10.1002/2017WR020467, 2017.

Ding, Y., Nie, Y., Chen, H., Wang, K., and Querejeta, J. I.: Water uptake depth is coordinated with leaf water potential, water-use efficiency and drought vulnerability in karst vegetation, New Phytologist, 229, 1339-1353, https://doi.org/10.1111/nph.16971, 2021.

Epstein, S. and Mayeda, T.: Variation of O18 content of waters from natural sources, Geochimica et Cosmochimica Acta, 4, 213-224, https://doi.org/10.1016/0016-7037(53)90051-9, 1953.

Estrada-Medina, H., Graham, R. C., Allen, M. F., Jiménez-Osornio, J. J., and Robles-Casolco, S.: The importance of limestone bedrock and dissolution karst features on tree root distribution in northern Yucatán, México, Plant and Soil, 362, 37-50, https://doi.org/10.1007/s11104-012-1175-x, 2013.

Evaristo, J., Jasechko, S., and McDonnell, J. J.: Global separation of plant transpiration from groundwater and streamflow,

Nature, 525, 91-94, https://doi.org/10.1038/nature14983, 2015.
Evaristo, J., McDonnell, J. J., and Clemens, J.: Plant source water apportionment using stable isotopes: A comparison of simple linear, two - compartment mixing model approaches, Hydrological Processes, 31, 3750 - 3758, https://doi.org/10.1002/hyp.11233, 2017.
Fabiani, G., Klaus, J., and Penna, D.: The influence of hillslope topography on beech water use: a comparative study in two different climates, Hydrol. Earth Syst. Sci., 28, 2683-2703, https://doi.org/10.5194/hess-28-2683-2024, 2024.
Fan, B., Xiong, K., and Liu, Z.: Forest Plant Water Utilization and the Eco-Hydrological Regulation in the Karst Desertification Control Drainage Area, Forests, 14, 747, https://doi.org/10.3390/f14040747, 2023.
Fan, Y. and Miguez-Macho, G.: Infiltration depth, rooting depth, and regolith flushing-A global perspective, PNAS Nexus, 3, pgae514, https://doi.org/10.1093/pnasnexus/pgae514, 2024.
Finkenbiner, C. E., Good, S., Brooks, J., Allen, S., and Sasidharan, S.: The physical basis for ecohydrologic separation: the roles of soil hydraulics and climate, https://doi.org/10.21203/rs.3.rs-1024190/v1, 2021.
Finkenbiner, C. E., Good, S. P., Renée Brooks, J., Allen, S. T., and Sasidharan, S.: The extent to which soil hydraulics can explain ecohydrological separation, Nature Communications, 13, 6492, https://doi.org/10.1038/s41467-022-34215-7, 2022.
Fu, H., Neil, E. J., Liu, J., and Si, B.: A Continuous Root Water Uptake Isotope Mixing Model, Water Resources Research, 60, e2023WR036852, https://doi.org/10.1029/2023WR036852, 2024.
Gai, H., Shi, P., and Li, Z.: Untangling the Uncertainties in Plant Water Source Partitioning With Isotopes, Water Resources Research, 59, e2022WR033849, https://doi.org/10.1029/2022WR033849, 2023.
Geris, J., Tetzlaff, D., McDonnell, J., Anderson, J., Paton, G., and Soulsby, C.: Ecohydrological separation in wet, low energy northern environments? A preliminary assessment using different soil water extraction techniques, Hydrological Processes, 29, 5139-5152, https://doi.org/10.1002/hyp.10603, 2015.
Hahm, W. J., Rempe, D. M., Dralle, D. N., Dawson, T. E., and Dietrich, W. E.: Oak Transpiration Drawn From the Weathered Bedrock Vadose Zone in the Summer Dry Season, Water Resources Research, 56, e2020WR027419, https://doi.org/10.1029/2020WR027419, 2020.
Hahm, W. J., Dralle, D. N., Sanders, M., Bryk, A. B., Fauria, K. E., Huang, M. H., Hudson-Rasmussen, B., Nelson, M. D., Pedrazas, M. A., Schmidt, L., Whiting, J., Dietrich, W. E., and Rempe, D. M.: Bedrock Vadose Zone Storage Dynamics Under Extreme Drought: Consequences for Plant Water Availability, Recharge, and Runoff, Water Resources Research, 58, e2021WR031781, https://doi.org/10.1029/2021WR031781, 2022.
Hartmann, A., Goldscheider, N., Wagener, T., Lange, J., and Weiler, M.: Karst water resources in a changing world: Review of hydrological modeling approaches, Reviews of Geophysics, 52, 218-242, https://doi.org/10.1002/2013RG000443, 2014.
Hasenmueller, E. A., Gu, X., Weitzman, J. N., Adams, T. S., Stinchcomb, G. E., Eissenstat, D. M., Drohan, P. J., Brantley, S. L., and Kaye, J. P.: Weathering of rock to regolith: The activity of deep roots in bedrock fractures, Geoderma, 300, 11-31, https://doi.org/10.1016/j.geoderma.2017.03.020, 2017.

He, K., Chen, X., Zhou, J., Zhao, D., and Yu, X.: Compound successive dry-hot and wet extremes in China with global warming and urbanization, Journal of Hydrology, 636, 131332, https://doi.org/10.1016/j.jhydrol.2024.131332, 2024.

Hervé-Fernández, P., Oyarzún, C., Brumbt, C., Huygens, D., Bodé, S., Verhoest, N. E. C., and Boeckx, P.: Assessing the 'two water worlds' hypothesis and water sources for native and exotic evergreen species in south-central Chile, Hydrological Processes, 30, 4227-4241, https://doi.org/10.1002/hyp.10984, 2016.

Howarth, F. and Bishop, B.: International Journal of Speleology Off icial Journal of Union Internationale de Spéléologie Why the delay in recognizing terrestrial obligate cave species in the tropics?, International Journal of Speleology, 52, https://doi.org/10.5038/1827-806X.52.1.2446, 2023.

Hubbert, K., Beyers, J., and Graham, R.: Roles of weathered bedrock and soil in seasonal water relations of Pinus Jeffreyi and Arctostaphylos patula, Canadian Journal of Forest Research, 31, 1947-1957, https://doi.org/10.1139/x01-136, 2011.

Jiang, Z., Liu, H., Wang, H., Peng, J., Meersmans, J., Green, S. M., Quine, T. A., Wu, X., and Song, Z.: Bedrock geochemistry influences vegetation growth by regulating the regolith water holding capacity, Nature Communications, 11, 2392, https://doi.org/10.1038/s41467-020-16156-1, 2020.

Jiménez-Rodríguez, C. D., Sulis, M., and Schymanski, S.: Exploring the role of bedrock representation on plant transpiration response during dry periods at four forested sites in Europe, Biogeosciences, 19, 3395-3423, https://doi.org/10.5194/bg-19-3395-2022, 2022.

Koeniger, P., Marshall, J. D., Link, T., and Mulch, A.: An inexpensive, fast, and reliable method for vacuum extraction of soil and plant water for stable isotope analyses by mass spectrometry, Rapid Communications in Mass Spectrometry, 25, 3041-3048, https://doi.org/10.1002/rcm.5198, 2011.

Korboulewsky, N., Tétégan, M., Samouelian, A., and Cousin, I.: Plants use water in the pores of rock fragments during drought, Plant and Soil, 454, 35-47, https://doi.org/10.1007/s11104-020-04425-3, 2020.

Landwehr, J. and Coplen, T. B.: Line-conditioned excess: a new method for characterizing stable hydrogen and oxygen isotope ratios in hydrologic systems, in, 132-135, 2006.

Leite, P. A. M., Rempe, D. M., McInnes, K. J., Schmidt, L. M., Walker, J. W., Olariu, H. G., and Wilcox, B. P.: Trees Enhance Rock Moisture Storage: A Major Pool in Karst Drylands and Crucial During Droughts, Water Resources Research, 61, e2024WR038692, https://doi.org/10.1029/2024WR038692, 2025.

Li, Y., Wang, S., Peng, T., Zhao, G., and Dai, B.: Hydrological characteristics and available water storage of typical karst soil in SW China under different soil–rock structures, Geoderma, 438, 116633, https://doi.org/10.1016/j.geoderma.2023.116633, 2023.

Lin, W., Wen, C., Wen, Z., and Gang, H.: Drought in Southwest China: A Review, Atmospheric and Oceanic Science Letters, 8, 339-344, https://doi.org/10.3878/AOSL20150043, 2015.

Liu, Q., Wang, T., Liu, C.-q., Mikouendanandi, E. M. R. B., Chen, X., Peng, T., and Zhang, L.: Characterizing the spatiotemporal dynamics of shallow soil water stable isotopic compositions on a karst hillslope in Southwestern China, Journal

of Hydrology, 610, 127964, https://doi.org/10.1016/j.jhydrol.2022.127964, 2022.

Liu, X.: Stable isotope ($\delta^{18}O$, δD) dataset of soil water, rock fracture water, precipitation, and xylem water in a subtropical karst ecosystem, southwest China (2022–2025), Zenodo [dataset], https://doi.org/10.5281/ZENODO.16810833, 2025.

Liu, X., Yue, F.-J., Wong, W. W., Guo, T.-L., and Li, S.-L.: Unravelling nitrate transformation mechanisms in karst catchments through the coupling of high-frequency sensor data and machine learning, Water Research, 267, 122507, https://doi.org/10.1016/j.watres.2024.122507, 2024a.

Liu, X., Liu, W., Chen, X., Wang, L., Zhang, Z., and Peng, T.: Estimating fracture characteristics and hydraulic conductivity from slug tests in epikarst of southwest China, Journal of Hydrology: Regional Studies, 53, 101777, https://doi.org/10.1016/j.ejrh.2024.101777, 2024b.

Liu, X., Chen, X., Zhang, Z., Liu, W., Gao, F., Cheng, Q., Chen, J., and Peng, T.: The Role of Rock Fractures as a Water Source for Trees Growing in Karst, Water Resources Research, 61, e2024WR039588, https://doi.org/10.1029/2024WR039588, 2025.

Liu, Y., Fang, Y., Hu, H., Tian, F., Dong, Z., and Khan, M. Y. A.: Ecohydrological Separation Hypothesis: Review and Prospect, Water, 12, 2077, https://doi.org/10.3390/w12082077, 2020.

Liu, Z., Liu, Z., Jia, G., Liu, Z., and Yu, X.: Employing stable isotopes to reveal temporal trajectories of water travelling through the soil – plant-atmosphere continuum, Journal of Hydrology, 644, 132058, https://doi.org/10.1016/j.jhydrol.2024.132058, 2024c.

Luo, J., Luo, W., Liu, J., Wang, Y., Li, Z., Tao, J., and Liu, J.: Karst fissures mitigate the negative effects of drought on plant growth and photosynthetic physiology, Oecologia, 205, 69-80, https://doi.org/10.1007/s00442-024-05556-5, 2024a.

Luo, Z., Fan, J., Shao, M., Yang, Q., and Li, M.: Rock moisture reinforces belowground water storage under different precipitation scenarios and vegetation coverage, Journal of Hydrology, 636, 131276, https://doi.org/10.1016/j.jhydrol.2024.131276, 2024b.

Luo, Z., Guan, H., Zhang, X., Xu, X., Dai, J., and Hua, M.: Examination of the ecohydrological separation hypothesis in a humid subtropical area: Comparison of three methods, Journal of Hydrology, 571, 642-650, https://doi.org/10.1016/j.jhydrol.2019.02.019, 2019.

Luo, Z., Nie, Y., Chen, H., Guan, H., Zhang, X., and Wang, K.: Water Age Dynamics in Plant Transpiration: The Effects of Climate Patterns and Rooting Depth, Water Resources Research, 59, e2022WR033566, https://doi.org/10.1029/2022WR033566, 2023.

Małoszewski, P. and Zuber, A.: Determining the turnover time of groundwater systems with the aid of environmental tracers: 1. Models and their applicability, Journal of Hydrology, 57, 207-231, https://doi.org/10.1016/0022-1694(82)90147-0, 1982.

McCole, A. A. and Stern, L. A.: Seasonal water use patterns of Juniperus ashei on the Edwards Plateau, Texas, based on stable isotopes in water, Journal of Hydrology, 342, 238-248, https://doi.org/10.1016/j.jhydrol.2007.05.024, 2007.

McCormick, E. L., Dralle, D. N., Hahm, W. J., Tune, A. K., Schmidt, L. M., Chadwick, K. D., and Rempe, D. M.: Widespread woody plant use of water stored in bedrock, Nature, 597, 225-229, https://doi.org/10.1038/s41586-021-03761-3, 2021.

McDonnell, J. J.: The two water worlds hypothesis: ecohydrological separation of water between streams and trees?, WIREs

Water, 1, 323-329, https://doi.org/10.1002/wat2.1027, 2014.

McGuire, K. J., DeWalle, D. R., and Gburek, W. J.: Evaluation of mean residence time in subsurface waters using oxygen-18 fluctuations during drought conditions in the mid-Appalachians, Journal of Hydrology, 261, 132-149, https://doi.org/10.1016/S0022-1694(02)00006-9, 2002.

Midwood, A. J., Boutton, T. W., Archer, S. R., and Watts, S. E.: Water use by woody plants on contrasting soils in a savanna parkland: assessment with δ2H and δ18O, Plant and Soil, 205, 13-24, https://doi.org/10.1023/A:1004355423241, 1998.

Moore, J. W. and Semmens, B. X.: Incorporating uncertainty and prior information into stable isotope mixing models, Ecology Letters, 11, 470-480, https://doi.org/10.1111/j.1461-0248.2008.01163.x, 2008.

Morrison, J., Brockwell, T., Merren, T., Fourel, F., and Phillips, A. M.: On-line high-precision stable hydrogen isotopic analyses on nanoliter water samples, Anal Chem, 73, 3570-3575, https://doi.org/10.1021/ac001447t, 2001.

Nardini, A., Tomasella, M., and Di Bert, S.: Bedrock: the hidden water reservoir for trees challenged by drought, Trees, 38, 1-11, https://doi.org/10.1007/s00468-023-02482-6, 2024.

Nardini, A., Petruzzellis, F., Marusig, D., Tomasella, M., Natale, S., Altobelli, A., Calligaris, C., Floriddia, G., Cucchi, F., Forte, E., and Zini, L.: Water 'on the rocks': a summer drink for thirsty trees?, New Phytologist, 229, 199-212, https://doi.org/10.1111/nph.16859, 2021.

Nie, Y.-p., Chen, H.-s., Wang, K.-l., and Yang, J.: Water source utilization by woody plants growing on dolomite outcrops and nearby soils during dry seasons in karst region of Southwest China, Journal of Hydrology, 420-421, 264-274, https://doi.org/10.1016/j.jhydrol.2011.12.011, 2012.

Ning, J., Liu, X., Wu, X., Yang, H., Ma, J., and Cao, J.: The Effect of Bedrock Differences on Plant Water Use Strategies in Typical Karst Areas of Southwest China, Land, 12, 12, https://doi.org/10.3390/land12010012, 2023.

Oshun, J., Dietrich, W. E., Dawson, T. E., and Fung, I.: Dynamic, structured heterogeneity of water isotopes inside hillslopes, Water Resources Research, 52, 164-189, https://doi.org/10.1002/2015WR017485, 2016.

Parnell, A. C., Phillips, D. L., Bearhop, S., Semmens, B. X., Ward, E. J., Moore, J. W., Jackson, A. L., Grey, J., Kelly, D. J., and Inger, R.: Bayesian stable isotope mixing models, Environmetrics, 24, 387-399, https://doi.org/10.1002/env.2221, 2013.

Parry, J. T.: The limestone pavements of northwestern England, Canadian Geographies 4, 14-21, https://doi.org/10.1111/j.1541-0064.1960.tb01836.x, 1960.

Pawlik, Ł., Phillips, J. D., and Šamonil, P.: Roots, rock, and regolith: Biomechanical and biochemical weathering by trees and its impact on hillslopes — A critical literature review, Earth-Science Reviews, 159, 142-159, https://doi.org/10.1016/j.earscirev.2016.06.002, 2016.

Peng, X., Dai, Q., Ding, G., Shi, D., and Li, C.: Impact of vegetation restoration on soil properties in near-surface fissures located in karst rocky desertification regions, Soil and Tillage Research, 200, 104620, https://doi.org/10.1016/j.still.2020.104620, 2020.

Peng, X., Wang, X., Dai, Q., Ding, G., and Li, C.: Soil structure and nutrient contents in underground fissures in a rock-mantled

slope in the karst rocky desertification area, Environmental Earth Sciences, 79, 3, https://doi.org/10.1007/s12665-019-8708-z, 2019.

Philip, J. R.: Plant Water Relations: Some Physical Aspects, Ann.rev.plant Physiol, 17, 245-268, 1966.

Preisler, Y., Tatarinov, F., Grünzweig, J. M., Bert, D., Ogée, J., Wingate, L., Rotenberg, E., Rohatyn, S., Her, N., Moshe, I., Klein, T., and Yakir, D.: Mortality versus survival in drought-affected Aleppo pine forest depends on the extent of rock cover and soil stoniness, Functional Ecology, 33, 901-912, https://doi.org/10.1111/1365-2435.13302, 2019.

Putman, A. L. and Bowen, G. J.: Technical Note: A global database of the stable isotopic ratios of meteoric and terrestrial waters, Hydrol. Earth Syst. Sci., 23, 4389-4396, https://doi.org/10.5194/hess-23-4389-2019, 2019.

Querejeta, J. I., Estrada-Medina, H., Allen, M. F., Jiménez-Osornio, J. J., and Ruenes, R.: Utilization of bedrock water by Brosimum alicastrum trees growing on shallow soil atop limestone in a dry tropical climate, Plant and Soil, 287, 187-197, https://doi.org/10.1007/s11104-006-9065-8, 2006.

Reddy, M. M., Schuster, P., Kendall, C., and Reddy, M. B.: Characterization of surface and ground water δ18O seasonal variation and its use for estimating groundwater residence times, Hydrological Processes, 20, 1753-1772, https://doi.org/10.1002/hyp.5953, 2006.

Rempe, D. M. and Dietrich, W. E.: Direct observations of rock moisture, a hidden component of the hydrologic cycle, Proceedings of the National Academy of Sciences, 115, 2664-2669, https://doi.org/10.1073/pnas.1800141115, 2018.

Rong, L., Chen, X., Chen, X., Wang, S., and Du, X.: Isotopic analysis of water sources of mountainous plant uptake in a karst plateau of southwest China, Hydrological Processes, 25, 3666-3675, https://doi.org/10.1002/hyp.8093, 2011.

Salomón, R. L., Peters, R. L., Zweifel, R., Sass-Klaassen, U. G. W., Stegehuis, A. I., Smiljanic, M., Poyatos, R., Babst, F., Cienciala, E., Fonti, P., Lerink, B. J. W., Lindner, M., Martinez-Vilalta, J., Mencuccini, M., Nabuurs, G.-J., van der Maaten, E., von Arx, G., Bär, A., Akhmetzyanov, L., Balanzategui, D., Bellan, M., Bendix, J., Berveiller, D., Blaženec, M., Čada, V., Carraro, V., Cecchini, S., Chan, T., Conedera, M., Delpierre, N., Delzon, S., Ditmarová, Ľ., Dolezal, J., Dufrêne, E., Edvardsson, J., Ehekircher, S., Forner, A., Frouz, J., Ganthaler, A., Gryc, V., Güney, A., Heinrich, I., Hentschel, R., Janda, P., Ježík, M., Kahle, H.-P., Knüsel, S., Krejza, J., Kuberski, Ł., Kučera, J., Lebourgeois, F., Mikoláš, M., Matula, R., Mayr, S., Oberhuber, W., Obojes, N., Osborne, B., Paljakka, T., Plichta, R., Rabbel, I., Rathgeber, C. B. K., Salmon, Y., Saunders, M., Scharnweber, T., Sitková, Z., Stangler, D. F., Stereńczak, K., Stojanović, M., Střelcová, K., Světlík, J., Svoboda, M., Tobin, B., Trotsiuk, V., Urban, J., Valladares, F., Vavrčík, H., Vejpustková, M., Walthert, L., Wilmking, M., Zin, E., Zou, J., and Steppe, K.: The 2018 European heatwave led to stem dehydration but not to consistent growth reductions in forests, Nature Communications, 13, 28, https://doi.org/10.1038/s41467-021-27579-9, 2022.

Salve, R., Rempe, D. M., and Dietrich, W. E.: Rain, rock moisture dynamics, and the rapid response of perched groundwater in weathered, fractured argillite underlying a steep hillslope, Water Resources Research, 48, https://doi.org/10.1029/2012WR012583, 2012.

Schoeman, J. L., Kruger, M. M., and Loock, A. H.: Water-holding capacity of rock fragments in rehabilitated opencast mine soils, South African Journal of Plant and Soil, 14, 98-102, https://doi.org/10.1080/02571862.1997.10635089, 1997.

Schwinning, S.: The ecohydrology of roots in rocks, Ecohydrology, 3, 238-245, https://doi.org/10.1002/eco.134, 2010.

Schwinning, S.: A critical question for the critical zone: how do plants use rock water?, Plant and Soil, 454, 49-56, https://doi.org/10.1007/s11104-020-04648-4, 2020.

Snelgrove, J. R., Buttle, J. M., Kohn, M. J., and Tetzlaff, D.: Co-evolution of xylem water and soil water stable isotopic composition in a northern mixed forest biome, Hydrol. Earth Syst. Sci., 25, 2169-2186, https://doi.org/10.5194/hess-25-2169-2021, 2021.

Sprenger, M. and Allen, S. T.: What Ecohydrologic Separation Is and Where We Can Go With It, Water Resources Research, 56, e2020WR027238, https://doi.org/10.1029/2020WR027238, 2020.

Sprenger, M., Leistert, H., Gimbel, K., and Weiler, M.: Illuminating hydrological processes at the soil-vegetation-atmosphere interface with water stable isotopes, Reviews of Geophysics, 54, 674–704, https://doi.org/10.1002/2015RG000515, 2016.

Sprenger, M., Llorens, P., Cayuela, C., Gallart, F., and Latron, J.: Mechanisms of consistently disjunct soil water pools over (pore) space and time, Hydrology and Earth System Sciences, 23, 2751-2762, https://doi.org/10.5194/hess-23-2751-2019, 2019.

Sprenger, M., Tetzlaff, D., Buttle, J., Laudon, H., Leistert, H., Mitchell, C. P. J., Snelgrove, J., Weiler, M., and Soulsby, C.: Measuring and Modeling Stable Isotopes of Mobile and Bulk Soil Water, Vadose Zone Journal, 17, 170149, https://doi.org/10.2136/vzj2017.08.0149, 2018.

Stewart, M. K. and McDonnell, J. J.: Modeling Base Flow Soil Water Residence Times From Deuterium Concentrations, Water Resources Research, 27, 2681-2693, https://doi.org/10.1029/91WR01569, 1991.

Stock, B. C. and Semmens, B. X.: Unifying error structures in commonly used biotracer mixing models, Ecology, 97, 2562-2569, https://doi.org/10.1002/ecy.1517, 2016.

Tang, K. and Feng, X.: The effect of soil hydrology on the oxygen and hydrogen isotopic compositions of plants' source water, Earth and Planetary Science Letters, 185, 355-367, https://doi.org/10.1016/S0012-821X(00)00385-X, 2001.

Tong, X., Brandt, M., Yue, Y., Horion, S., Wang, K., Keersmaecker, W. D., Tian, F., Schurgers, G., Xiao, X., Luo, Y., Chen, C., Myneni, R., Shi, Z., Chen, H., and Fensholt, R.: Increased vegetation growth and carbon stock in China karst via ecological engineering, Nature Sustainability, 1, 44-50, https://doi.org/10.1038/s41893-017-0004-x, 2018.

Vargas, A. I., Schaffer, B., Yuhong, L., and Sternberg, L. d. S. L.: Testing plant use of mobile vs immobile soil water sources using stable isotope experiments, New Phytologist, 215, 582-594, https://doi.org/10.1111/nph.14616, 2017.

Vrettas, M. D. and Fung, I. Y.: Sensitivity of transpiration to subsurface properties: Exploration with a 1-D model, Journal of Advances in Modeling Earth Systems, 9, 1030-1045, https://doi.org/10.1002/2016MS000901, 2017.

Wang, H., Yu, H., He, D., Li, M., Si, B., McDonnell, J. J., and Nehemy, M. F.: Cryogenic vacuum distillation vs Cavitron methods in ecohydrology: Extraction protocol effects on plant water isotopic values, Journal of Hydrology, 642, 131853,

https://doi.org/10.1016/j.jhydrol.2024.131853, 2024a.

Wang, J., Lu, N., and Fu, B.: Inter-comparison of stable isotope mixing models for determining plant water source partitioning, Sci Total Environ, 666, 685-693, https://doi.org/10.1016/j.scitotenv.2019.02.262, 2019a.

Wang, K., Liu, Z., Zeng, T., Wang, F., Shen, W., and Shao, J.: Performance of enhanced geothermal system with varying injection-production parameters and reservoir properties, Applied Thermal Engineering, 207, 118160, https://doi.org/10.1016/j.applthermaleng.2022.118160, 2022.

Wang, K., Zhang, C., Chen, H., Yue, Y., Zhang, W., Zhang, M., Qi, X., and Fu, Z.: Karst landscapes of China: patterns, ecosystem processes and services, Landscape Ecology, 34, 2743-2763, https://doi.org/10.1007/s10980-019-00912-w, 2019b.

Wang, L., Cardenas, M. B., Slottke, D. T., Ketcham, R. A., and Sharp Jr., J. M.: Modification of the Local Cubic Law of fracture flow for weak inertia, tortuosity, and roughness, Water Resources Research, 51, https://doi.org/10.1002/2014WR015815, 2015.

Wang, P., Song, X., Han, D., Zhang, Y., and Liu, X.: A study of root water uptake of crops indicated by hydrogen and oxygen stable isotopes: A case in Shanxi Province, China, Agricultural Water Management, 97, 475-482, https://doi.org/10.1016/j.agwat.2009.11.008, 2010.

Wang, S., Yan, Y., Zhao, Y., Fu, Z., and Chen, H.: Co-evolution among soil thickness, epikarst weathering degree, and runoff characteristics on a subtropical karst hillslope, Journal of Hydrology, 628, 130499, https://doi.org/10.1016/j.jhydrol.2023.130499, 2024b.

Wei, S., Chu, X., Sun, B., Yuan, W., Song, W., Zhao, M., Wang, X., Li, P., and Han, G.: Climate warming negatively affects plant water-use efficiency in a seasonal hydroperiod wetland, Water Research, 242, 120246, https://doi.org/10.1016/j.watres.2023.120246, 2023.

Williams, P. W.: The role of the epikarst in karst and cave hydrogeology: a review, International Journal of Speleology, 37, 1-10, http://dx.doi.org/10.5038/1827-806X.37.1.1, 2008.

Wolfsberg, A.: Rock Fractures and Fluid Flow: Contemporary Understanding and Applications, Eos, Transactions American Geophysical Union, 78, 569-573, https://doi.org/10.1029/97EO00345, 1997.

Wu, H., Fan, H., Li, J., Yue, F.-J., Lian, E., Fu, C., Lei, R., Ding, M., Liu, J., and Li, X.-Y.: Reproducing surface water isoscapes of δ 18O and δ 2H across China: A machine learning approach, Journal of Hydrology, 638, 131565, https://doi.org/10.1016/j.jhydrol.2024.131565, 2024a.

Wu, Z., Behzad, H. M., He, Q., Wu, C., Bai, Y., and Jiang, Y.: Seasonal transpiration dynamics of evergreen Ligustrum lucidum linked with water source and water-use strategy in a limestone karst area, southwest China, Journal of Hydrology, 597, 126199, https://doi.org/10.1016/j.jhydrol.2021.126199, 2021.

Wu, Z., Lv, T., Zeng, S., Zhang, X., Wu, H., Luo, S., Bai, Y., Zhang, Y., and Jiang, Y.: Differential responses in water-use strategies of evergreen (Ligustrum lucidum) and deciduous (Robinia pseudoacacia) trees to tunnel excavation in a subtropical karst trough valley, Journal of Hydrology, 636, 131323, https://doi.org/10.1016/j.jhydrol.2024.131323, 2024b.

Xu, W., Xia, X., Piao, S., Wu, D., Li, W., Yang, S., and Yuan, W.: Weakened Increase in Global Near-Surface Water Vapor

Pressure During the Last 20 Years, Geophysical Research Letters, 51, e2023GL107909, https://doi.org/10.1029/2023GL107909, 2024.

Xu, X., Zhao, Z., and Skrzypek, G.: Stable isotope disequilibrium between soil bound water and soil bulk water – Implications for estimations of plant water sources, Journal of Hydrology, 650, 132544, https://doi.org/10.1016/j.jhydrol.2024.132544, 2025.

Xu, X., Yan, Y., Dai, Q., Yi, X., Hu, Z., and Cen, L.: Spatial and temporal dynamics of rainfall erosivity in the karst region of southwest China: Interannual and seasonal changes, CATENA, 221, 106763, https://doi.org/10.1016/j.catena.2022.106763, 2023.

Yan, Y., Yang, Y., and Dai, Q.: Effects of preferential flow on soil nutrient transport in karst slopes after recultivation, Environmental Research Letters, 18, 034012, https://doi.org/10.1088/1748-9326/acb8cc, 2023.

Yang, J., Nie, Y., Chen, H., Wang, S., and Wang, K.: Hydraulic properties of karst fractures filled with soils and regolith materials: Implication for their ecohydrological functions, Geoderma, 276, 93-101, https://doi.org/10.1016/j.geoderma.2016.04.024, 2016.

Younger, S. E., Blake, J., Jackson, C. R., and Aubrey, D. P.: δ2H isotopic offsets in xylem water measurements under cryogenic vacuum distillation: Quantifying and correcting wood-water hydrogen exchange influences, Ecohydrology, 17, e2640, https://doi.org/10.1002/eco.2640, 2024.

Zeng, X., Xu, X., Yi, R., Zhong, F., and Zhang, Y.: Sap flow and plant water sources for typical vegetation in a subtropical humid karst area of southwest China, Hydrological Processes, 35, e14090, https://doi.org/10.1002/hyp.14090, 2021.

Zhang, F. and Zhang, C.: Probing water partitioning in unsaturated weathered rock using nuclear magnetic resonance, Geophysics, 86, WB131-WB147, https://doi.org/10.1190/geo2020-0591.1, 2021.

Zhang, J., Wang, J., Chen, J., Song, H., Li, S., Zhao, Y., Tao, J., and Liu, J.: Soil Moisture Determines Horizontal and Vertical Root Extension in the Perennial Grass Lolium perenne L. Growing in Karst Soil, Frontiers in Plant Science, Volume 10 - 2019, https://doi.org/10.3389/fpls.2019.00629, 2019a.

Zhang, Y., Zhang, M., Niu, J., Li, H., Xiao, R., Zheng, H., and Bech, J.: Rock fragments and soil hydrological processes: Significance and progress, CATENA, 147, 153-166, https://doi.org/10.1016/j.catena.2016.07.012, 2016.

Zhang, Y., Ge, H., Liu, G., Shen, Y., Chen, H., Wang, J., Liu, D., and Huang, Z.: Experimental Study of Fracturing Fluid Retention in Rough Fractures, Geofluids, 2019, 2603296, https://doi.org/10.1155/2019/2603296, 2019b.

Zhang, Z., Chen, X., Cheng, Q., and Soulsby, C.: Using StorAge Selection (SAS) functions to understand flow paths and age distributions in contrasting karst groundwater systems, Journal of Hydrology, 602, 126785, https://doi.org/10.1016/j.jhydrol.2021.126785, 2021.

Zhao, Y. and Wang, L.: Insights into the isotopic mismatch between bulk soil water and Salix matsudana Koidz trunk water from root water stable isotope measurements, Hydrol. Earth Syst. Sci., 25, 3975-3989, https://doi.org/10.5194/hess-25-3975-2021, 2021.

Zhao, Z., Deng, J., Zhang, J., and Shen, Y.: Effects of Film-Mulched Rock Outcrops on Rainwater Redistribution and Maize

Growth in the Cropland of a Rocky Karst Area, Water, 16, 254, https://doi.org/10.3390/w16020254, 2024.

Zhou, L., Wang, X., Wang, Z., Zhang, X., Chen, C., and Liu, H.: The challenge of soil loss control and vegetation restoration in the karst area of southwestern China, International Soil and Water Conservation Research, 8, 26-34, https://doi.org/10.1016/j.iswcr.2019.12.001, 2020.

Zimmerman, R. W. and Bodvarsson, G. S.: Hydraulic conductivity of rock fractures, Transport in Porous Media, 23, 1-30, https://doi.org/10.1007/BF00145263, 1996.

Zwieniecki, M. A. and Newton, M.: Roots growing in rock fissures: Their morphological adaptation, Plant and Soil, 172, 181-187, https://doi.org/10.1007/BF00011320, 1995.

Zwieniecki, M. A. and Newton, M.: Water-Holding Characteristics of Metasedimentary Rock in Selected Forest Ecosystems in Southwestern Oregon, Soil Science Society of America Journal, 60, 1578-1582, https://doi.org/10.2136/sssaj1996.03615995006000050042x, 1996.